Progress in Surface Science xxx (xxxx) xxx–xxx

Contents lists available at ScienceDirect

Progress in Surface Science

journal homepage: www.elsevier.com/locate/progsurf

Review article

Water at surfaces and interfaces: From molecules to ice and bulk liquid

Tomoko K. Shimizu[a], Sabine Maier[b], Albert Verdaguer[c], Juan-Jesus Velasco-Velez[d], Miquel Salmeron[e,*]

[a] Department of Applied Physics and Physico-Informatics, Faculty of Science and Technology, Keio University, 3-14-1 Hiyoshi, Kohoku-ku, Yokohama, Kanagawa 223-8522, Japan
[b] Department of Physics, Friedrich-Alexander-Universität Erlangen-Nürnberg, Erwin-Rommel-Str. 1, 91058 Erlangen, Germany
[c] Institut de Ciència de Materials de Barcelona ICMAB-CSIC, Campus de la UAB, E-08193 Bellaterra, Spain
[d] Department of Inorganic Chemistry, Fritz-Haber-Institute der Max-Planck-Gesellschaft, Berlin 14195, Germany
[e] Materials Science Division, Lawrence Berkeley National Laboratory, and Materials Science and Engineering Dept., University of California, Berkeley, USA

ABSTRACT

The structure and growth of water films on surfaces is reviewed, starting from single molecules to two-dimensional wetting layers, and liquid interfaces. This progression follows the increase in temperature and vapor pressure from a few degrees Kelvin in ultra-high vacuum, where Scanning Tunneling and Atomic Force Microscopies (STM and AFM) provide crystallographic information at the molecular level, to ambient conditions where surface sensitive spectroscopic techniques provide electronic structure information. We show how single molecules bind to metal and non-metal surfaces, their diffusion and aggregation. We examine how water molecules can be manipulated by the STM tip via excitation of vibrational and electronic modes, which trigger molecular diffusion and dissociation. We review also the adsorption and structure of water on non-metal substrates including mica, alkali halides, and others under ambient humid conditions. We finally discuss recent progress in the exploration of the molecular level structure of solid-liquid interfaces, which impact our fundamental understanding of corrosion and electrochemical processes.

1. Introduction

Water/solid interfaces are of fundamental interest in various fields including geology, metrology, biology, and chemistry. Despite its simple molecular structure, the structure and interactions of water with surfaces, which determines wetting and reactivity, remain unsolved. The knowledge of this structure at the nanoscale is crucial to understand key properties that determine corrosion, dissolution, and electrochemical processes. Comprehensive review papers on water/solid interfaces were published in 1987 by Thiel and Maday [1] and in 2002 by Henderson [2]. Studies by Auger electron spectroscopy (AES), electron energy loss spectroscopy (EELS), infrared reflection absorption spectroscopy (IRAS), X-ray photoelectron spectroscopy (XPS), low energy electron diffraction (LEED), and temperature-programmed desorption (TPT) and many others were covered. Studies using scanning probe microscopies (SPM) were also discussed in Ref. [2]. One of the differences of SPM from other techniques is the locality of the information. SPM uses a probe tip to scan over the surface, and obtain structural information together with, e.g., electronic, mechanical, and vibrational properties. Because it is not an averaged information over a wide area, as in the case of all the other techniques listed above, detailed investigations of how atomic steps, kinks, and defects residing on the surface influence on the adsorption of molecules are possible.

There has been a great amount of progress since that time which we try to review, including the studies related to SPM. With scanning tunneling microscopy (STM) operated under ultra-high vacuum (UHV) and low temperature, we can observe not only

* Corresponding author.
E-mail address: mbsalmeron@lbl.gov (M. Salmeron).

https://doi.org/10.1016/j.progsurf.2018.09.004

structures of adsorbed water molecules, but also vibrational signals through inelastic electron tunneling (IET) processes, which are closely related to water diffusion and dissociation. Because these are the phenomena observed in UHV, to bridge the pressure gap, other types of SPM based on mechanic or electromagnetic forces have been developed that make possible to image in ambient conditions. They are known by a variety of names: atomic force microscopy (AFM) and its variants of contact and non-contact, lateral force microscopy, and attractive electrostatic force microscopies, known as scanning polarization force microscopy (SPFM) and Kelvin Probe Force Microscopy (KPFM). The non-contact attractive AFM modes allow us to observe water films formed on solids with minimal disruption.

We will first discuss adsorption configurations, diffusion, aggregation, and dissociation of water on metal surfaces induced thermally, vibrationally and electronically using STM. These topics were reviewed also by Hodgson and Haq in 2009 [3] from the theoretical point of view. We then move to formation of larger clusters and monolayers. The discussion of the "ice" layers is followed by liquid water films minerals (salts, oxides) in ambient conditions. In the last section, we also review recent studies of liquid water near a solid, electrified surface. Here the knowledge obtained from X-ray absorption spectroscopy (XAS) has proved useful for better understanding of atomistic pictures of electrochemical processes.

2. Single molecules: diffusion, aggregation, dissociation

2.1. Water on metal surfaces at low coverage: monomers and small clusters

STM studies of adsorption of water on metal surfaces started in the early 2000s, with noble metals, including Au, Ag, Cu, and more reactive transition metals, such as Pt, Pd, Rh, Ru have been used as substrates.

The first observation of individual water molecules was reported in 2001 by Lauhon and Ho [4] on Cu(0 0 1) using low-temperature STM. They pointed out several phenomena occurring during imaging of adsorbed water: (1) stable clusters form at relatively low coverage, (2) imaging of small clusters (less than 6 molecules) often leads to tip induced molecular motions, and (3) large clusters have internal structures that are often difficult to resolve.

Morgenstern et al. [5–9] studied water adsorption at 70 K on Ag(1 1 1). They found that cyclic hexamers are the smallest stable unit. Based on their 3-fold symmetric appearance the authors proposed configurations in which three of six molecules lie flat on the surface while the other three are positioned with one hydrogen pointing-up. Later, in 2007, the same group came up with a new interpretation based on better-resolved images, backed up with density functional theory (DFT) calculations [10].

On metals where water molecules bind more strongly, such as Pd and Ru, the presence of water monomers was reported. On Pd (1 1 0), Komeda et al. [11] found 3 types of protrusions with different heights at the coverage of 0.02 ML. The temperature during the adsorption of water was estimated to be below 50 K, high enough for diffusion but not for dissociation. The smallest protrusions, 15 pm high, were attributed to water monomers and the highest to tetramers. However, the identification of these species based only on imaging is difficult. As shown later, excitation of specific vibrations that induce motions and reactions are key to unambiguous identification.

On Pd(1 1 1) at 40 K, Fomin et al. [12] showed, based on STM images resolving both the Pd lattice and the water monomers, that the adsorption site was the on-top site of the Pd. Similarly, on Ru(0 0 0 1), Shimizu et al. [13] showed that H_2O deposited at 25 K appeared as a round protrusion with a height ranging from 50 to 65 pm at the on-top site (Fig. 1a–c). Ab-initio calculations revealed that the highest occupied molecular orbital (HOMO; state $1B_1$) and the second lowest unoccupied molecular orbital (LUMO + 1; state $2B_2$) interact significantly with the Ru atoms. This leads to a non-negligible projected density of states (PDOS) of water at the Fermi level that causes a positive contrast. The contributions of molecular orbitals to the tunneling current is 45% of HOMO, giving the rounded shape, 37% of LUMO + 1, and −18% (negative contribution) of $2A_1$, which distort the circular symmetry (Fig. 1d). The remaining 32% of tunneling current is due to direct tunneling into the Ru atoms surrounding the atom directly in contact with the water molecule. When the water monomer was trapped by a residual carbon impurity, residing at an hcp hollow site, the height was found to decrease to 20–35 pm. The reduction of height was explained by the electronic effect arising from the formation of the hydrogen bond.

The above picture agrees with a theoretical study by Michaelides et al. [14] who calculated the energy of water monomers adsorbed on closed-packed metals, including Rh(1 1 1), Ru(0 0 0 1), Pt(1 1 1), Pd(1 1 1), Cu(1 1 1), Ag(1 1 1), and Au(1 1 1). The adsorption energies rank high to low in that order from 0.42 eV to 0.13 eV. It should be noted that the calculation of the adsorption energy for Au(1 1 1) did not take into account the herring-bone reconstruction, and thus water at the elbow site observed in the experiment [15] should be adsorbed more strongly. The molecular orbital (MO) contributions to water binding on these surfaces were found to be similar: the delocalized $1B_1$ MO interacts with metal wave functions yielding the so-called "flat-lying" configuration, where the molecular dipole vectors and OH bonds are nearly parallel to the surface. The round appearance of the monomer in the STM images is the result of its rapid rotation at a finite temperature. Árnadóttir et al. calculated the rotation barriers to be as low as 10 meV on Pt(1 1 1) [16].

Motobayashi et al. [17,18] studied water monomers and dimers on Pt(1 1 1). After deposition of H_2O or D_2O below 20 K, they observed two types of protrusions in the STM images: one circular and the other with "flower-shape", assigned to monomers and dimers respectively. The flower-shapes were shown to be dimers by manipulating and bringing together two monomers. The appearance was explained as due to one water molecule on a top site acting as a donor, and the other as acceptor hoping around it. Similar flower-shaped species were also found on Ru(0 0 0 1) [19]. The energy barrier for the rotation of the acceptor molecule around the donor molecule was found to be ~20 meV by DFT calculation [16], which is slightly smaller than half the energy of the hindered lateral rotation modes of the acceptor molecule. Therefore, the zero-point energy of the hindered rotational modes is

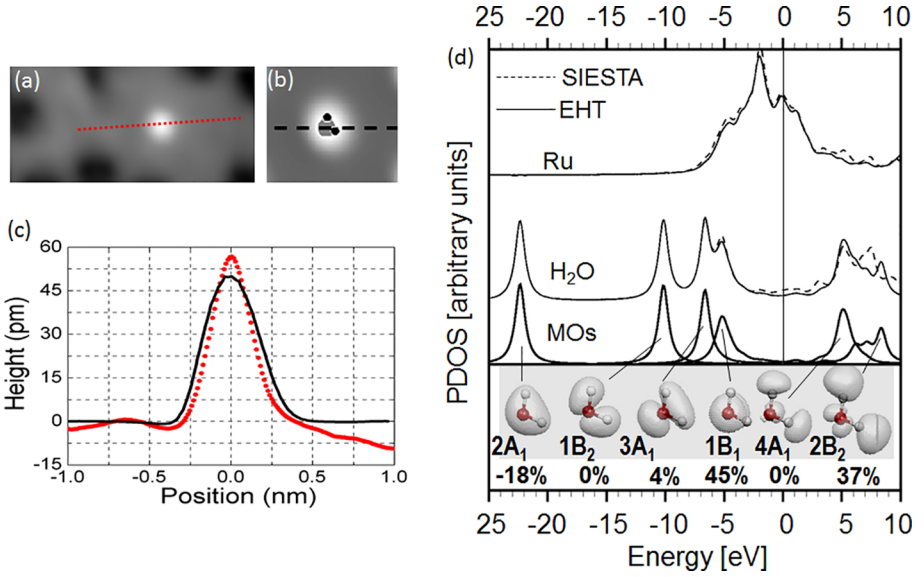

Fig. 1. Water monomer adsorption on Ru(0 0 0 1). (a) STM image (3 nm x 1.4 nm) showing an isolated water monomer (bright spot) as a protrusion. Dark hollows are residual carbon impurity atoms. (b) Simulated STM image of a water monomer. (c) Experimental (red) and theoretical (black) height profiles taken from (a) and (b). (d) Density of states (DOS) for the Ru(0 0 0 1)-$p(4 \times 4)$ + H_2O system projected (PDOS) onto the H_2O molecule and the Ru atom below it. Reprinted with permission from [13]. Copyright 2008 American Chemical Society. (For interpretation of the references to color in this figure legend, the reader is referred to the web version of this article.)

enough to excite rotation of the acceptor. It also implies that the variation of adsorption energy near the on-top site is quite small, allowing for the formation of ($\sqrt{37} \times \sqrt{37}$) and ($\sqrt{39} \times \sqrt{39}$) structures upon formation of a monolayer. Water layer structures will be discussed in detail in the next section.

2.2. Diffusion of monomers to form dimers and small clusters

Diffusion of the adsorbed molecules leads to aggregation, bonding, and reactions with other surface species. The behavior of water diffusion can be observed using STM at low temperatures when the thermal energy is small enough to slow down the molecular movement. At 40 K on Pd(1 1 1), an interesting and unexpectedly fast diffusion of dimers was found, four orders of magnitude higher than that of monomers. Mitsui et al. [20] observed diffusion and aggregation of small clusters of H_2O, with the monomer colliding first with another monomer to produce a dimer. The dimer further diffused and encountered a third monomer to form a trimer. Finally, the trimer collided with other molecules to form pentamers and hexamers. These two structures were stable without further diffusion at this temperature (Fig. 2). A possible explanation of the faster dimer diffusion was proposed by Ranea et al. [21]. Their DFT calculations suggested that the role of the donor and the acceptor is successively exchanged by quantum tunneling of the H-atom when the two molecules bind metastably to the metal atoms. As a result, the dimer moves in a rotation that resembles a “couple dancing a waltz”. If this mechanism is correct a much slower diffusion of D_2O dimers should be observed. Such an experiment, however, has not been performed thus far.

2.3. Manipulation of water molecules: Tip-induced diffusion and rotation

Fomin et al. [12] studied the vibrationally-assisted diffusion of H_2O and D_2O monomers on Pd(1 1 1). When the energy of the tunneling electron exceeded the energy of the scissor mode, ~200 meV for H_2O and ~150 meV for D_2O, the hopping rate of the monomers increased dramatically. Based on the tunneling current dependence of the hopping rate, the authors concluded that the process was a single-electron vibrational excitation of the scissor mode, which anharmonically couples to frustrated translation modes of the water molecule. Excitation of the scissor mode was also found to induce diffusion of water clusters on Cu(1 1 1) [7].

On Ru(0 0 0 1), the higher binding energy of water and the concomitantly higher diffusion barrier required excitation of the more energetic O-H stretching mode to induce hopping of H_2O monomers. Mugarza et al. [19] studied possible tip-induced processes of H_2O at 6 K. They observed diffusion, desorption, and transfer to the tip after applying voltage pulses of 450–550 mV, but no increase in diffusion rate by excitation of the scissor mode. The current dependence of the hopping rate suggested a 1 electron process for isolated H_2O, similar to the Pd(1 1 1) case.

Tip-induced diffusion of dimers on Pt(1 1 1) was studied by Motobayashi et al. [17]. As explained in the previous section, the water dimer appears as a “flower-shape,” and is stable enough to be observed at 5 K. From *I*(tunneling current)-*t*(time) plots while the tip is above the central donor molecule at various bias voltages, they drew an “action” spectrum, which is a plot of yield of event vs. bias voltage (Fig. 3). They obtained spectra for monomers and dimers of H_2O and D_2O. Spectral fitting revealed a correspondence of

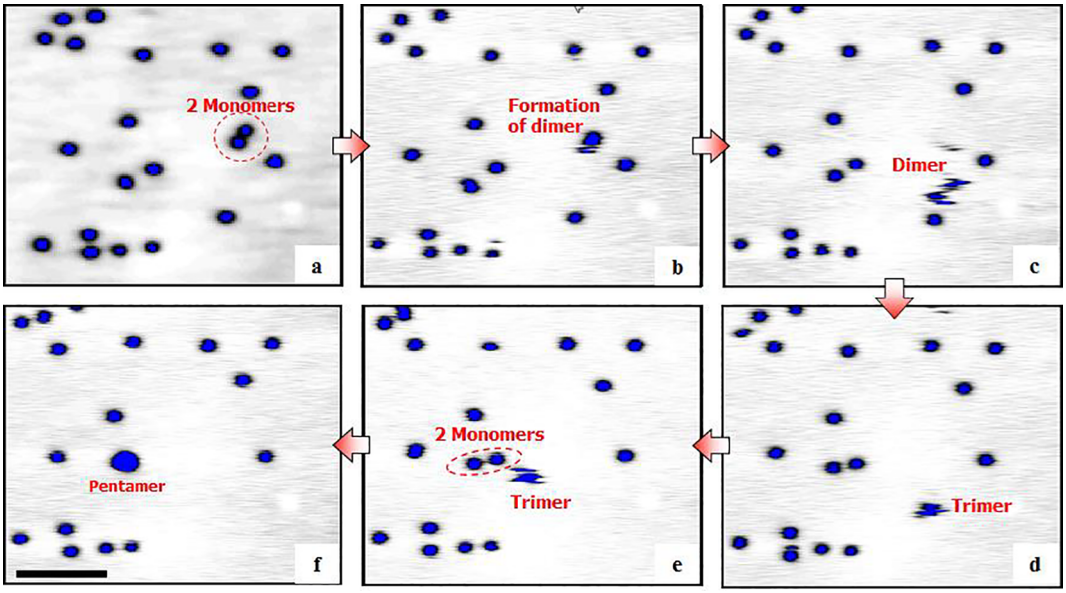

Fig. 2. Sequential STM images ($V_s = -100$ mV, $I_t = 150$ pA) showing diffusion and clustering of water on Pd(1 1 1). The scale bar represents 0.5 nm. Reprinted with permission from [20].

the increase in yield with vibrational modes involved. For H_2O dimer excitation increases were found at energies corresponding to: (1) the scissor mode, (2) combination of the scissor mode and O-Pt stretch mode of the donor, (3) combination of the scissor mode and H-O-Pt libration mode of the donor, and (4) OH stretch mode of the donor that participates in a hydrogen bond. In contrast, for D_2O three energies were found: (1) OD stretch mode of the donor that participates in a hydrogen bond, (2) OD stretch mode of the acceptor pointing toward the Pt surface, and (3) free OD stretch mode of the donor. By comparing with theoretically obtained energy values for two different configurations, H (of the acceptor)-down and H-parallel, the authors concluded that the H or D from OH(OD) of the acceptor molecule should point toward the Pt surface, forming a hydrogen bond. The study also showed that the hopping of both monomers and dimers is achieved by one-electron processes, and the diffusion barrier of the dimers is greater than that of the monomers. This trend agrees with a theoretical study by Árnadóttir et al. [22], though the absolute values of diffusion barriers were about two times larger than the experimental values. As discussed earlier, the diffusion barrier of the dimer was found to be much smaller than that of a monomer on Pd(1 1 1). The difference between the two substrates may be due to a different diffusion mechanism, although the answer is unknown at this moment.

2.4. Manipulation of water molecules: Tip-induced dissociation

In addition to diffusion, excitation of vibrational modes of water by tunneling electrons can induce dissociation reactions. Dissociation of water occurs either in two steps, by sequential abstraction of hydrogen atoms, or in a single step, directly to atomic oxygen. In both cases, observation of the dissociated H atoms products is quite rare as they easily diffuse far away from the reaction site.

On metal surfaces such as Ru(0 0 0 1) [19], Cu(1 0 0) [4], and Cu(1 1 0) [23], a ladder-type single quanta excitation of the O-H stretch mode cannot rupture the O-H bond within the experimental parameters. Instead, when a single electron has enough energy to excite several quanta of the O-H stretch mode, above 1.5 V, water can be dissociated [19]. After a voltage pulse at this energy, the appearance of water changed to a faint protrusion with an apparent height of ~10 pm on Ru(0 0 0 1), which was attributed to OH species. This OH diffuses readily even at a bias voltage as low as 150 mV, and the diffusion is induced inelastically by the excitation of low energy modes such as frustrated translations and librations. When the bias voltage of the pulse was increased above 2 V, OH could be dissociated, the O atom being observed as a negative contrast (depression) in STM images. An important point is that only a positive sample bias can induce these dissociation reactions. This polarity dependence indicates that electronic excitation to an antibonding state is responsible for the dissociation process.

An interesting comparison can be made with the case of Cu surfaces. Lauhon et al. [4] found that dissociation thresholds for H_2O and OH on Cu(1 0 0) were 1.5 and 4 eV, respectively, a similar trend to Ru(0 0 0 1) [19]; however, diffusion of OH species required excitation of the O-H stretch mode [4], higher energy than the case on Ru(0 0 0 1). On Cu(1 1 0), surprisingly the necessary voltage to induce OH dissociation is 0.9 V, smaller than 2.0 V for dissociation from H_2O to OH [23]. It is clear that the potential landscapes are completely different for different surfaces, making prediction of the energy required for dissociation for various substrates challenging.

In the above cases, multiple quanta excitation of the vibrational mode to induce reactions was not achieved, but it was observed with water adsorbed on an insulator. Shin et al. [24] studied water adsorption on MgO(1 0 0) films formed on Ag(1 0 0) at 4.7 K.

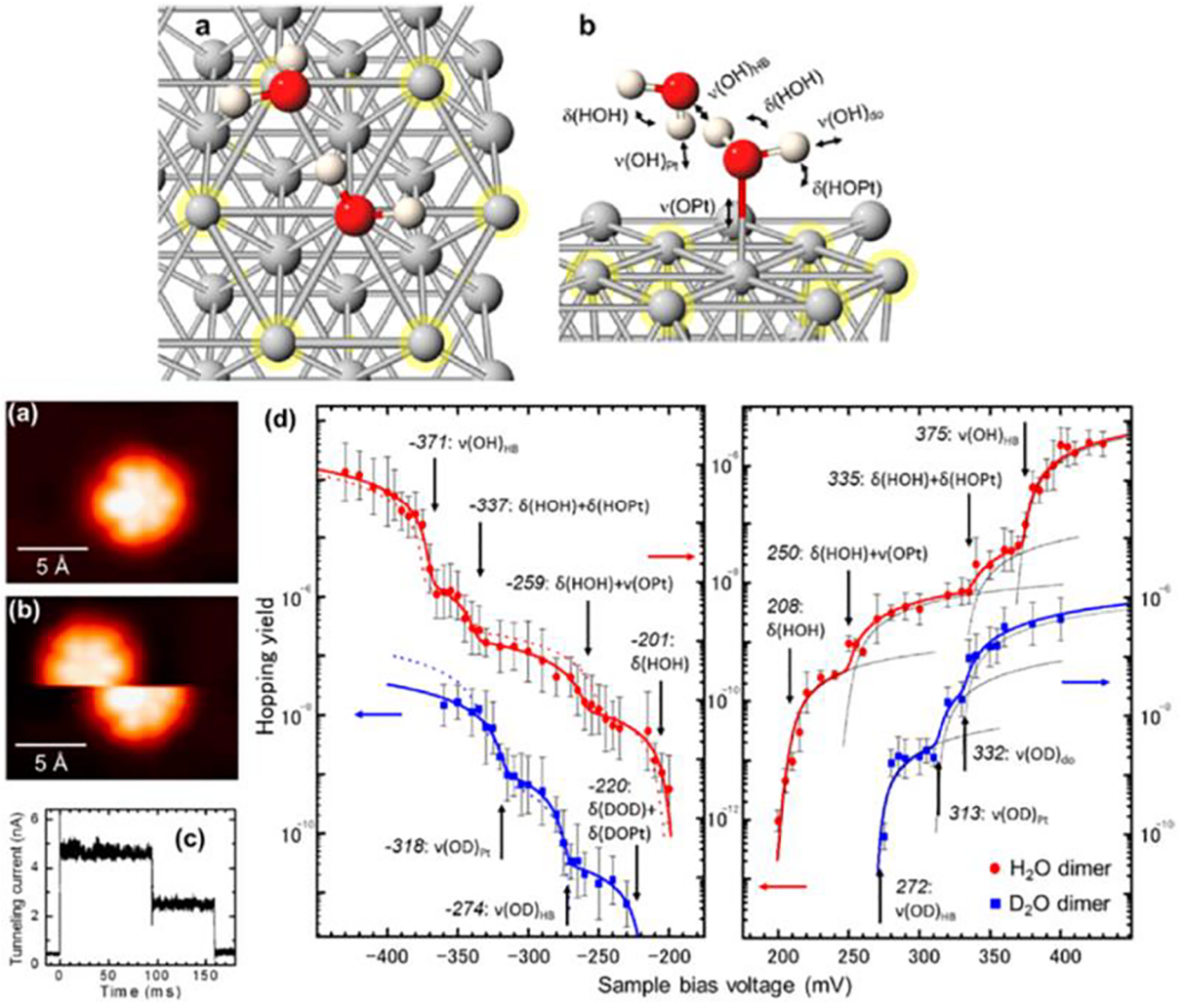

Fig. 3. Upper panel: Top view (a) and side view (b) of the optimized structure of a water dimer on Pt(1 1 1). The involved vibrational modes are indicated in (b). Lower panel: (a) STM image (V_s = 40 mV, I_t = 1.0 nA) of a H_2O dimer on Pt(1 1 1). (b) STM image (V_s = 40 mV, I_t = 1.0 nA) of the H_2O dimer when lateral hopping was induced by a voltage pulse at 250 mV and 5 nA for 1 s. (c) The tunneling current measured as a function of time under constant applied voltage (280 mV, 160 ms). The step indicates the occurrence of a molecular motion. (d) STM-action spectra (AS) and spectral fit of the lateral hopping of H_2O and D_2O dimers on Pt(1 1 1) at positive (right) and negative (left) sample bias voltages. The red circles and blue squares represent the experimental results of the STM-AS for H_2O and D_2O, respectively. Reprinted with permission from [17]. Copyright 2014 American Chemical Society. (For interpretation of the references to color in this figure legend, the reader is referred to the web version of this article.)

Insertion of the insulating film extends the lifetime of an electron in the excited molecular state, making the inelastic electron tunneling process much more efficient than on metals. This allows dissociation of H_2O to OH with a bias voltage at 450 mV via sequential excitations of the O-H stretch mode (Fig. 4a–c). When a bias voltage above 1.5 V was applied, dissociation products appeared to be atomic oxygen (Fig. 4d–e). The electronic excitation to the LUMO level allowed complete dissociation of water in a single event, which is also different from the case of water adsorbed on metallic substrates.

3. From single molecules to wetting layers

3.1. Formation of the first water layer

Water hexamer rings are energetically more stable as compared to the dimer units on Pd(1 1 1) and Ru(0 0 0 1) [25,26]. DFT calculations predict that the hexamers adopt a planar structure on reactive surfaces, such as Pd(1 1 1) and Ru(0 0 0 1) [27], while on Cu and Ag [10] the hexamers are buckled, owing to a weaker surface interaction. Upon further water addition at 130 K the molecules attach to the vertices of the hexamers, as seen for Ru(0 0 0 1) in Fig. 5a. Subsequently, metastable clusters of limited size grow with peculiar shapes in the form of chains (see Fig. 5b) or rosette structures consisting of seven water hexagonal rings (see Fig. 5d), as

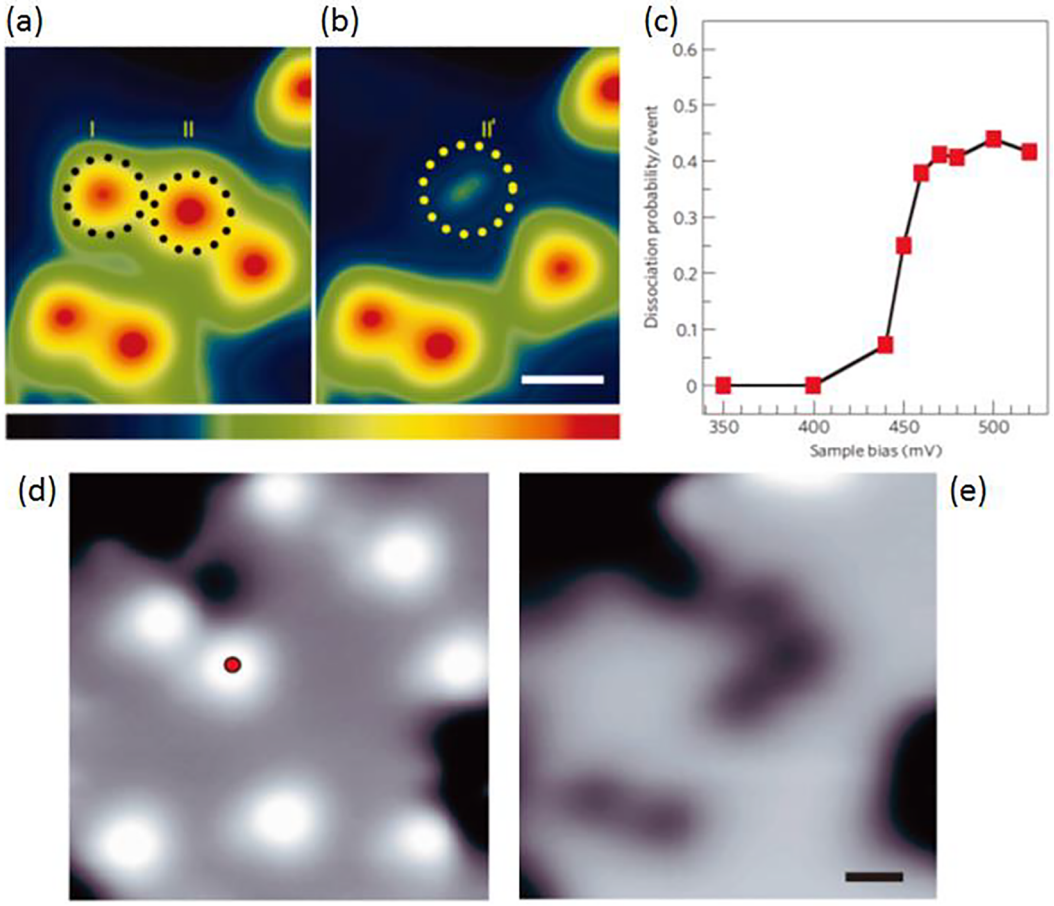

Fig. 4. Comparison of dissociation of water on MgO(1 0 0)/Ag(1 0 0) via vibrational excitation (a–c) and electronic excitation (d–e). (a) and (b) STM images (V_s = 50 mV and I_t = 0.3 nA) of water molecules before (a) and after (b) applying a bias voltage of 460 mV with tunneling currents of 3 nA and 5 nA at I and II, respectively. (c) The dissociation probability of isolated water molecules. The probability was derived from the ratio of the number of dissociated molecules to the total number of trials (~20) at each bias, maintaining the constant tunneling current of 5 nA and pulse duration of 400 μs. (d–e) STM images (V_s = 100 mV and I_t = 0.3 nA) of before (d) and after (e) dissociation of water by applying a bias voltage of 1.5 V. The scale bars represent 1 nm. Reprinted with permission from [24]. Copyright 2010 Nature Publishing Group.

observed on Ru(0 0 0 1) [27,28] and Pd(1 1 1) [25], respectively. The growth of these peculiar size-limited clusters on hexagonal close-packed surfaces proceeds according to a proposed two-dimensional ice rule [25,27]. The rules postulate that water molecules adsorb in a nearly flat geometry, binding to the metal via the O atom on top sites. This allows the molecules to form a honeycomb network by donating two H-bonds to neighboring molecules and accepting one. However, the imbalance of acceptor and donor sites in two-dimensional structures limits the number of hexamers that can be connected in this geometry. The growth of larger islands requires that some water molecules with a single donor or double acceptor geometry are included into the clusters in order to maintain an H-bonded network. Double acceptor/single donor molecules are rotated such that their plane is nearly vertical, either with H-up or H-down configuration, hence losing the strong bonding to the metal surface from the O-lone pair electrons. Rosette- and chain-type structures allow for the majority of water molecules to adsorb flat, in contrast to extended layers, and can thus maximize the water-surface bonding by minimizing the number of uncoordinated H atoms [25].

At higher water coverage, islands of connected hexagons with high- and low-lying domains formed on Ru(0 0 0 1) and Pd(1 1 1). They show a peculiar structure in the molecularly-resolved STM images, as shown in Fig. 5c [29]. The hexagons in the high-lying domains are rotated by 30° with respect to those in the low-lying areas due to the incorporation of double acceptor molecules. The molecules in the high-lying domains have a weaker interaction with the metal surface. Pentagonal and heptagonal rings mediate the transition between high- and low-lying domains. This growth mode is not limited to small clusters but was first found in extended water films deposited on Pt(1 1 1) by Ni et al. [30]. These non-hexagonal wetting-layers are a consequence of the optimization of the water-surface interaction, where in the low-lying hexagonal rings the water molecules bound to top sites of the close-packed metal lattice without breaking the hydrogen-bonded network. This has also been observed in other close-packed metal substrates, including Ru(0 0 0 1) [29] and Ni(1 1 1) [31]. While on Ru(0 0 1) and Pd(1 1 1) no-long order has been observed in these non-hexagonal wetting layers by STM [29], large unit cells with a (√37 × √37)R25.3° and (√39 × √39)R16.1° supercells are formed on Pt(1 1 1) [30] and a (7 × 7) on Ni(1 1 1) [31].

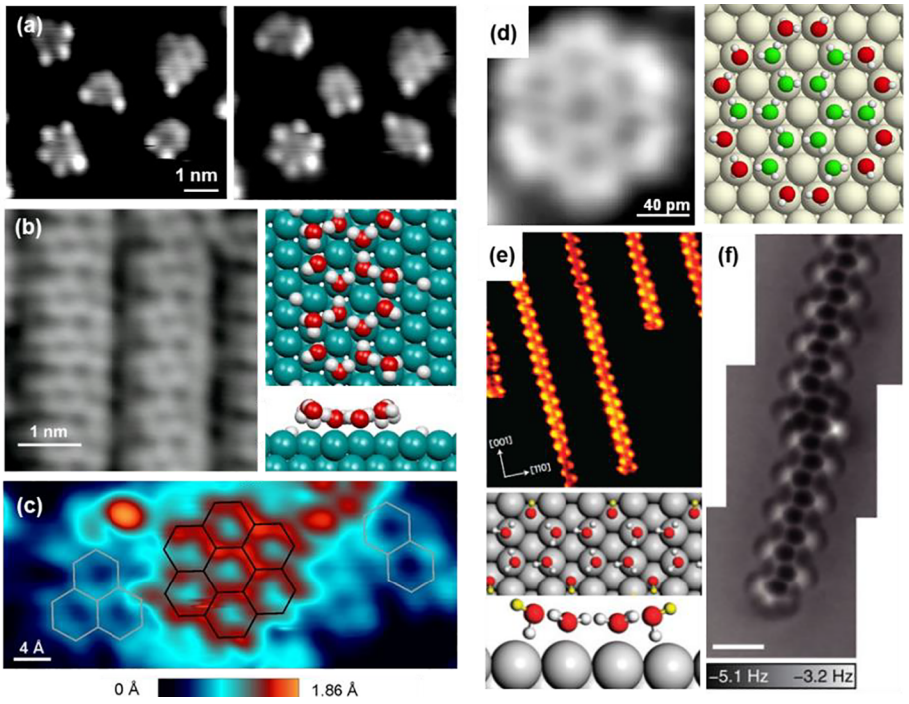

Fig. 5. Water cluster on various metal substrates: (a) Sequence of two STM images showing the motion of attached water molecules at the vertices of water hexamers on Ru(0 0 0 1) at 50 K; (b) STM image and corresponding DFT model of chains composed of hexamers on Ru(0 0 0 1); (c) Small water clusters with rotated water hexamers on Ru(0 0 0 1); (d) STM image and DFT model of a rosette-type water cluster on Pd(1 1 1); (e) STM image (12 nm × 14 nm), DFT and (f) nc-AFM measurements (scale bar 1 nm) of chains composed of water pentamers on Cu(1 1 0). (a) Reprinted with permission from Ref. [27], copyright 2009, ACS; (b) reprinted with permission from Ref. [28], copyright 2014, APS; (c) reprinted with permission from Ref. [29], copyright 2012, APS; (d) Reprinted with permission from Ref. [25], copyright 2004, APS; (e) Reprinted with permission from Ref. [35], copyright 2009, Nature Materials; (f) Reprinted with permission from Ref. [36], copyright 2017, Nature Communications.

STM studies in conjunction with DFT of water wetting layers on close-packed metal surfaces showed that water forms complex structures to optimize the molecule-surface interaction that are far from the “ice-like” bilayer model, which has been the standard model of water adsorption on close-packed metals in the 1980s and 1990s. The bilayer model assumed that water forms a hexagonal H-bonded network stabilized by weak molecule-surface interactions. Döring and Madey [32] proposed that water molecules in this ice-like layer forms structures similar to those of the (0 0 0 1) basal plane in ice *Ih*, consisting of a buckled 2D hexagonal network, where half of the water molecules are bound to the metal via the oxygen lone pair orbital, while the other half is lifted from the surface and H-bonded to the first half in a pseudo-tetrahedral arrangement. Thereby, uncoordinated H atoms of the water are oriented either away from the surface (“H-up”) or pointing “H-down” towards the metal, see Fig. 6. The numerous surface science studies on water wetting layers on metals were motivated by the DFT calculations of Feibelman who questioned the “ice-like” bilayer model [33]. He revealed that the adsorption energy of intact water layers on Ru(0 0 0 1) is too low and suggested that the wetting layer is stabilized by partial dissociation of the water molecules into hydroxyl groups that are hydrogen bonded in a hexagonal structure. The water dissociation is an activated process on Ru(0 0 0 1), which as will be discussed in the next paragraph.

Recently, water adsorption has also been studied on non-hexagonal metals surfaces as well as alloys [34]. For instance, the (1 1 0) surfaces are ideal templates for the formation of extended water chains. On Cu(1 1 0), the chains are composed of pentamers with four flat water molecules adsorbed on top sites that are completed by one tilted molecule in a double H-bond acceptor configuration, as observed by STM, nc-AFM, and DFT (Fig. 5e–f) after adsorption at 100 K and 78 K, respectively [35,36]. The short atomic spacing of the metal atoms hinders the formation of hexamer rings, which would require a lateral compression by ~1 Å of the ring for water to sit in the favored atop site. The extended chains run perpendicular to the close-packed Cu rows and get progressively closer until they become unstable upon increasing the water coverage until a continuous hexagonal 2D water film forms [37]. DFT calculations suggest that pentamer chains would also be favored on Ni(1 1 0) while hexamer chains would be more stable on Ag(1 1 0) and Pd (1 1 0) [35].

3.2. Thermally driven water dissociation on metal surfaces

On Ru(0 0 0 1), adsorbed water undergoes partial dissociation upon annealing, producing OH and H. This is an activated process with a dissociation barrier near that for desorption, as first evidenced by XPS [38] and DFT [39]. Therefore, water forms intact metastable structures at low temperatures while electron or X-ray irradiation [38,40–42] as well as annealing above 104–150 K

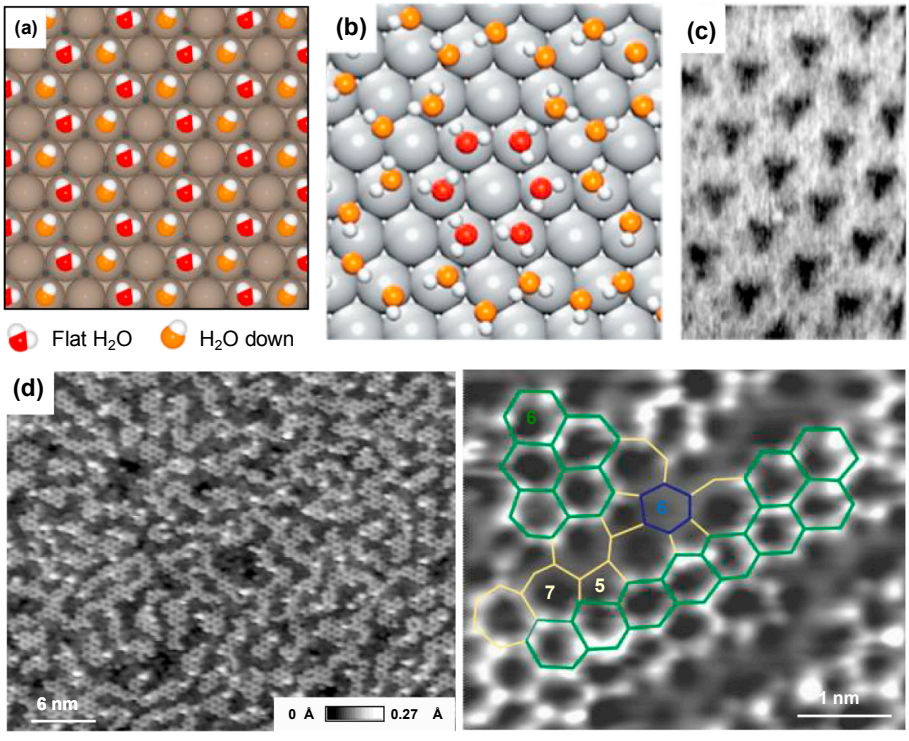

Fig. 6. Extended water layers on hexagonal close-packed metal substrates. (a) Schematics is showing a model of an "ice-like" bilayer on a close-packed metal surface. (b)–(c) DFT structure and STM image (7 nm × 10 nm) of a monolayer water on Pt(1 1 1) exhibiting a (√37 × √37)R25.3° reconstruction after deposition of submonolayer amounts of water at 140 K. (d) H_2O wetting layer on Ru(0 0 0 1) with high-lying (rotated, bright) and low-lying (in registry, dark) water domains after annealing at 140 K. In the magnified image (right) the rotated hexagons (marked by blue and green lines) are connected by pentagonal and heptagonal rings. Reprinted with permission from (b)–(c) Ref. [30], copyright 2010, APS and (d) Ref. [29], copyright 2012, APS. (For interpretation of the references to color in this figure legend, the reader is referred to the web version of this article.)

[40–43] induces partial dissociation. Accordingly, the narrow stripes that are composed of intact water molecules and follow the 2D water rules (Fig. 5b) transform into mixed water-hydroxyl stripes (Fig. 7b) which are rotated by 30° with respect to the intact ones [28]. The partially dissociated water stripes are composed of hexagonal rings of molecular water and hydroxyl species and have a width that varies from one to three or four hexagonal ring units, corresponding to around 2.5–6 Ru lattice constants, see (Fig. 7a) [28,41]. Ratios of H_2O:OH ranging from 3:1 to 4:0, with an average of roughly 5:3 [28,41], are suggested by a comparison of STM data and DFT calculations, which agrees with XPS data [40,44]. The OH groups are primarily embedded within the hexagonal chains, enabling the structure to stay flat and maximize the amount of water bonding flat to top Ru sites. The driving force for the stripe formation is the hydrogen liberated during the dissociation process, which prefers to adsorb on the Ru fcc sites between the H_2O-OH stripes. Occasionally, dark spots inside the rings suggest H atoms were observed, similar to those predicted by Feibelman [33]. The reorientation of the stripes was explained by the maximization of the number of dissociated molecules that can be accommodated, as opposed to an optimization of the hydrogen-bond density [28].

The efficiency of water dissociation depends strongly on the catalyst. On many oxide surfaces, water dissociates forming a variety of hydroxyl groups and hydroxyl-*water* complexes. On metals, water dissociation occurs readily on the active metals like Fe but the reactivity decreases in the more noble metals [2]. For example, on the clean, hexagonal close-packed Pt-group metal surfaces, only on the Rh(1 1 1) hydroxyl structures have been observed [44]. However, surface steps and defects may alter the chemical reactivity for water dissociation, as shown experimentally by STM experiments and DFT calculations on Pt(1 1 1). Thereby, water adsorption and reactions depend on the particular geometry of the steps, (1 0 0) vs. (1 1 1) type [45]. Water does not dissociate on clean Pt(1 1 1), but DFT calculations by Donadio et al. [46] showed that water chains at the (1 1 1) type steps of Pt(2 2 1) preferably partially dissociate. In contrast, Kolb et al. [47] observed that water remains intact on (1 1 1) steps but should partially dissociate on the more open (1 0 0) type steps.

3.3. Co-adsorption of water with other species

It is known that impurities, in particular chemisorbed oxygen, can facilitate water dissociation ($O + H_2O \rightarrow 2OH$). Therefore, many coadsorption studies have been carried out employing surface science techniques, in particular, water coadsorbed with alkali atoms, O_2 and CO [2]. For instance, hydroxyl can be formed by pre-dosing the surface with oxygen, which reacts with water to form mixed OH/H_2O layers [48,49]. This reaction is facile on many surfaces and occurs at temperatures below 150 K on Pt(1 1 1) and Pd

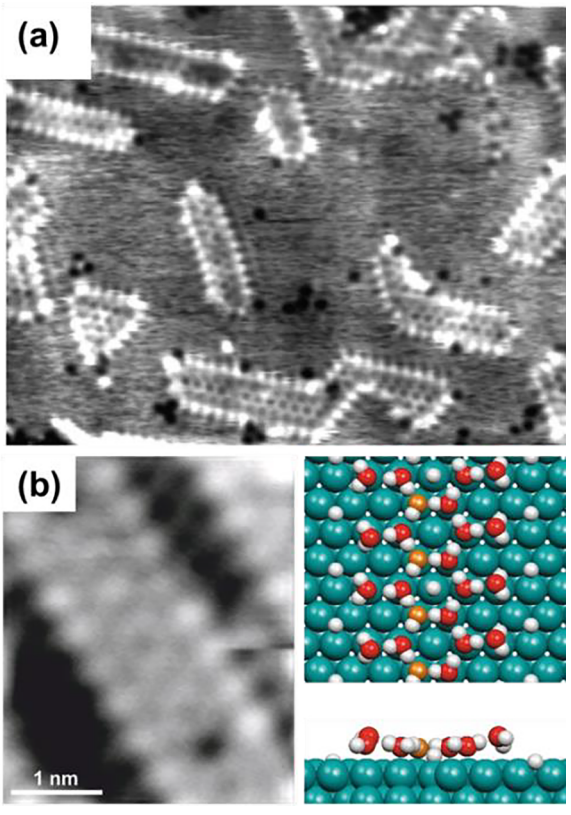

Fig. 7. Partial dissociation of H_2O on Ru(0 0 0 1). (a) STM image (200 × 160 Å^2) of partially dissociated water structures formed by dosing 3–4 ML of H_2O at 45 K and subsequent annealing to 180 K. (b) Partially dissociated H_2O-OH stripes after 30 min annealing at 145 K. Occasionally dark spots are seen in the center of the hexagons that correspond to trapped H atoms. In the DFT optimized structures, the OH groups are highlighted by orange O atoms. (a) Reprinted with permission from Ref. [41], copyright 2008, AIP and (b) Ref. [28], copyright 2014, APS. (For interpretation of the references to color in this figure legend, the reader is referred to the web version of this article.)

(1 1 1), to produce chemisorbed OH. In contrast, STM and XPS experiments have shown that only at low oxygen coverage partial dissociation of H_2O occurs on Ru(0 0 0 1) [50,51]. At oxygen coverages between 0.25 (O(2 × 2)) and 0.50 ML (O(2 × 1)) dissociation is inhibited. The intact water molecules are bound to Ru top sites via the O lone pair and stabilized by H-bonds to neighboring O atoms, see Fig. 8a [50–54]. At higher O coverage when all top sites are blocked, the adsorbed water causes a shift of half of the oxygen atoms from hcp sites to fcc sites, which creates a honeycomb structure such that water molecules bind strongly to the exposed Ru atoms [54]. DFT revealed that the energy cost of reconstructing the oxygen overlayer is more than compensated by the adsorption energy of water on the newly exposed Ru atoms.

As part of an effort to understand solvation phenomena, recently molecular layers of water on Pt(1 1 1) were produced subsequently exposed to NH_3 [55]. The NH_3 causes water molecules to rotate to expose an H atom that forms a hydrogen bond with the NH_3 molecule. Most notably, such a process proceeds with zero energy barrier, as shown by DFT.

3.4. From water monolayers to ice films

Since water-surface interactions strongly influence the structure of the interface, unraveling the structure of the first water layer is the first step towards the understanding of the water-solid interface. However, it is expected that water-water interactions dominate the growth of thicker layers and the transition to ice-like structures. For example, the wetting layers discussed above with rotated hexagonal domains, possess no dangling OH groups, and thus are not suitable to stabilize ice multilayers [56]. Therefore, the structure of the first water layer is expected to change upon adsorption of further water to allow the growth of thicker ice films.

The growth of water multilayers strongly depends on the preparation procedure. Amorphous solid water films form at low temperatures, in a metastable form due to the low mobility of water. At higher temperatures (> 120–160 K) the amorphous layers can transform into multilayer ice crystallites, which was first observed by Kimmel et al. by rare gas physisorption experiments [57,58]. Low-temperature STM experiments revealed that on Pt(1 1 1) and Ru(0 0 0 1) the amorphous ice structures grow in a layer by layer mode [59,60]. At 140 K, STM measurements showed the formation of flat multilayer ice crystallites alongside water monolayers, see Fig. 9a [60,61]. Thereby, the first layer water on Pt(1 1 1) changes to a (√3 × √3)R30° structure to optimize the interaction with subsequent multi-layers [62]. From the observations of screw-dislocations above the site of Pt steps in STM Fig. 9b, it

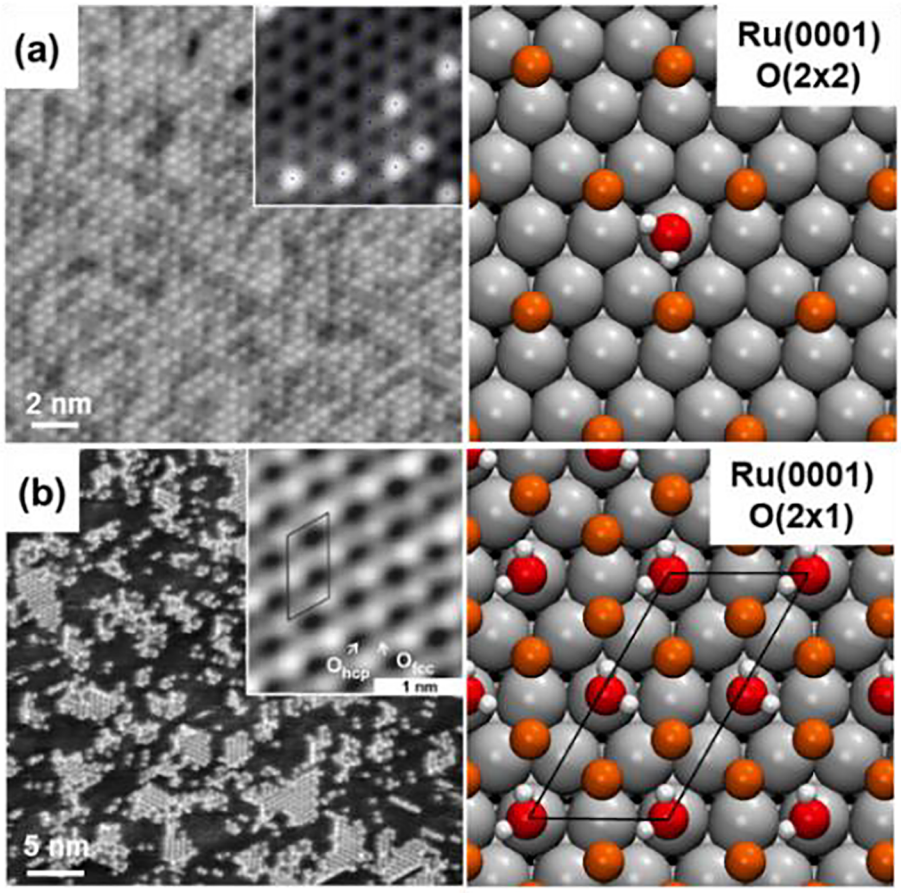

Fig. 8. STM images (left) and calculated structures (right) of water adsorbed on the (a) O(2 × 2) and (b) O(2 × 1) Ru(0 0 0 1) surface. Water molecules adsorb intact with the O bound to Ru top sites and the H atoms forming H-bonds to the neighboring O atoms in the lattice. Adapted from (a) Ref. [52] and (b) Ref. [54], © 2010 APS.

was concluded that cubic ice *Ic* is kinetically favored during rapid growth to avoid the need for nucleation of a new ice layer on the surface instead of forming the stable ice *Ih* [60,63]. A restructuring of the water interface layer during growth of 3D crystalline ice was also observed on Ni(1 1 1) [31] and Ru(0 0 0 1) [59]. An atomic-level understanding of crystalline water multilayers was provided on Ru(0 0 0 1) [59] by STM, see Fig. 9c–e. Besides the restructuring of the first layer, the molecular structure of domain boundaries between ice domains was resolved. The structure consists of pairs of five-membered rings separated by eight-membered rings as shown in Fig. 9e. Such planar defects may facilitate the formation of stacking faults, coinciding with a change from ice *Ih* to metastable cubic ice *Ic* as concluded by recent MD calculations [64].

In contrast, on the more hydrophobic Cu(1 1 1) surface water forms 3D clusters, with a variety of complex structures, but never perfect *Ih* or *Ic* ice terminations [65]. Instead, monomer-decorated double bilayers with different superstructures, a faceted surface, and pyramidal islands and nanocrystallites were identified by STM, depending on the coverage. Instead of the simple bilayer termination, a (2 × 1) superstructure and pyramidal facets of *Ih*(1 1 0 1) or *Ic*(2 2 1) are the most commonly observed terminating motifs of water clusters on Cu(1 1 1).

3.5. Water on metal oxide surfaces at low coverages

So far, we mostly discuss water adsorbed on clean metallic surfaces. This is because STM is powerful for conducting surfaces. Studies of water adsorbed on oxidized surfaces are more challenging, but have attracted increasing attention due to recent advances in noncontact atomic force microscopy [66]. We will review briefly here studies of water on oxides and salts in form of ultra-thin films of sub-nanometer thickness, which have been studied by SPM probes in ultra-high vacuum conditions. The more practical case of thick oxides, minerals, and bulk salt crystals is reviewed in the next sections.

Ultra-thin films of insulators such as NaCl and MgO can be formed on metallic surfaces in UHV, and water monomers and clusters adsorbed on these surfaces have been studied. Because the adsorption energy is very small, deposition at low temperature is necessary. In some cases tip functionalization is needed to obtain images with good resolution. One of such examples is water adsorbed on NaCl film/Au(1 1 1). The group of Jiang observed molecular orbitals of monomers and tetramers, from which they found

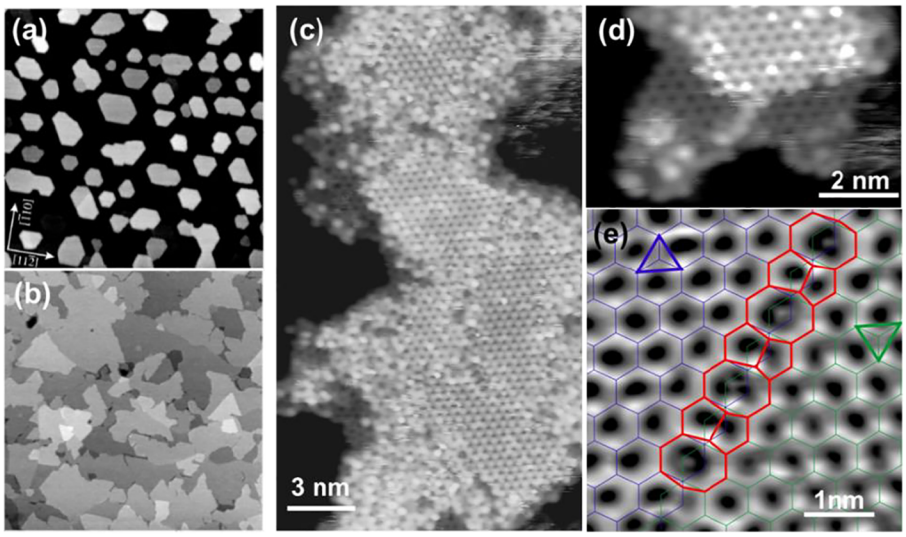

Fig. 9. Water multilayers on close-packed metal surfaces: (a) STM image of individual 3 nm high ice crystals grown on Pt(1 1 1) at 140 K, 500 nm × 500 nm. (b) Surface image of a continuous 4 nm thick ice film grown onto on Pt(1 1 1) at 140 K, 750 nm × 750 nm. (c)–(e) Molecularly-resolved STM images of a crystalline ice cluster containing two water layers surrounded by exposed Ru(0 0 0 1). (e) STM image showing a defect line of five- and eight-membered ring motifs in a two-layer ice film on Ru(0 0 0 1). (a) Reprinted with permission from Ref. [61], copyright 2008, APS; (b) Reprinted with permission from Ref. [60], copyright 2008, APS; (c)–(e) Reprinted with permission from Ref. [59], copyright 2016, ACS.

hydrogen-bond directionality [67]. Using a Cl ion functionalized tip, the group demonstrated concerted proton tunneling within the cyclic tetramer [68] and hydrogen bond strength of water monomers using inelastic electron tunneling spectroscopy (IETS) [69]. Diffusion of water monomers on NaCl/Ag(1 1 1) were studied by Heidorn et al. [70], where they obtain the diffusion barrier energy, the pre-exponential factor, and the attempt frequency. Based on these values, they proposed a diffusion mechanism and pointed out the influence of the metal substrate.

Besides monomers, water clusters and ordered overlayers have also been investigated on various semiconductor metal oxide surfaces with various surface science methods [1,2]. The adsorption of water on oxide surfaces in general is more complex, because the water molecules do not only interact with the metal cations but also with the oxygen anions. On these surfaces water molecules exhibit stronger interactions, which usually facilitate the dissociation of the molecule due to the presence of defects and co-ordinatively unsaturated metal cations. The understanding of the interactions and reactions of water on TiO_2 surfaces for example, was extensively studied by averaging techniques and local probes [71]. Recently, investigations have also been carried out to understand the water interaction of perovskite oxides at the molecular level. For instance, Halwidl et al. have studied the adsorption of water on the SrO-terminated surface of strontium ruthenates, $Sr_{n+1}Ru_nO_{3n+1}$, which consist of *n* layers of perovskite-like $SrRuO_3$ [72]. For a detailed review on structural motifs of water on metal oxide surfaces, we refer the reader to Ref. [71].

4. Water on bulk mineral and salt surfaces in ambient conditions

4.1. Water on mica

The study of water interaction with mineral, biological, and polymer surfaces is important because these materials are the most common in our world. Most of the studies are based on the use of SPM combined with a variety of other techniques. An example of the use of complementary techniques can be found in a work of Summer et al. [73] who used contact angle, IR, AFM and XPS measurements to study water uptake on different hydrophilic and hydrophobic surfaces such as glass, quartz, Teflon, and self-assembled organic monolayers (SAM). The general trend observed is that up to 60% relative humidity water forms films less than 5 molecules thick, even on very hydrophilic surfaces. In the rest of this section, we will review a subset of studies on these complex surfaces, focusing on water on mineral surfaces at ambient conditions of temperature and relative humidity. While AFM in its various operation modes is a powerful technique, imaging water near ambient conditions is challenging due to the easy perturbation of the water layers by the AFM probe. Several techniques have been developed to overcome these problems and a good summary can be found in Ref. [74].

The first technique used to image water films on mica was called Scanning Polarization Force Microscopy (SPFM), based on the application of DC or AC voltages to the tip and measurement of the deflection of the lever due to the electrostatic force (see schematic in Fig. 10). When using a second feedback where a DC voltage is applied to compensate the contact potential difference between tip and surface during imaging the technique is also called Kelvin Potential Force Microscopy (KPFM). In SPFM/KPFM the tip is typically a few nanometers above the surface, which minimizes disruptions of the water film at the cost of reduced spatial resolution. The first application of SPFM was to study the film formed by condensation of water on mica in equilibrium with vapor, by Hu et al. [75]. The

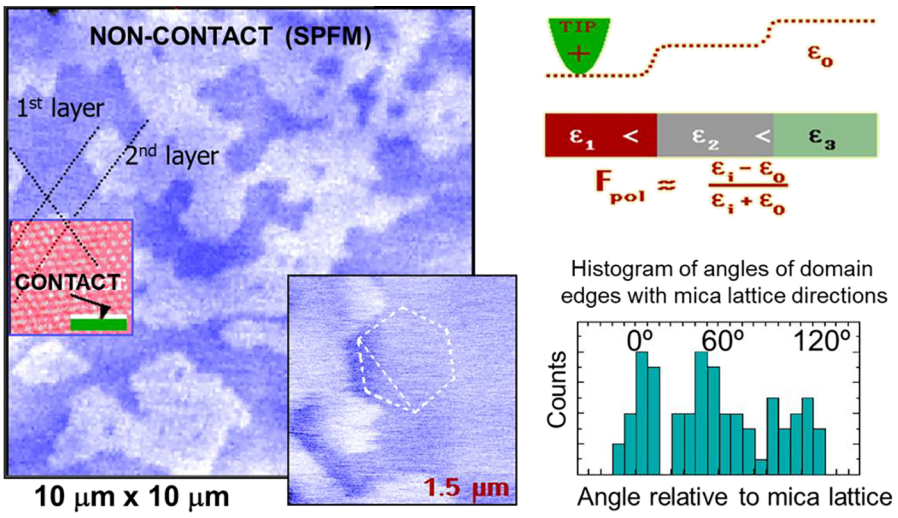

Fig. 10. Schematic of the operation of SPFM based on measuring the electrostatic force between the tip and the surface. The force is determined not only by the tip-sample distance but also by the materials dielectric constant. Left: SPFM image of water structures formed on mica in equilibrium with vapor at RT. The brighter islands are from a second layer film, with boundaries of polygonal shape, as shown more clearly in the smaller inset image (a hexagon is drawn for visual reference). The directions are strongly correlated with the mica lattice. The smaller inset (red, on the left), shows a contact AFM image obtained after acquisition of the non-contact SPFM images. A histogram of the angles of the boundaries of the water islands relative to the mica lattice is shown at the bottom right. (For interpretation of the references to color in this figure legend, the reader is referred to the web version of this article.)

authors found that mono- and bi-layers of water grow epitaxially oriented relative to the mica lattice, as shown in Fig. 10, which suggest an ice-like structure. Using Sum Frequency Generation (SFG), a non-linar optical spectroscopy where visible and infrared photons are combined and re-emitted in non-centro symmetric sites such as those present in surfaces, it was shown that the molecules in the first layer have all their hydrogen atoms forming H-bonds with other molecules or with O atoms of the substrate. The second layer, however, was found to grow with exposed or dangling H atoms [76]. These conclusions were further supported by measurements of the surface contact potential using SPFM. The contact potential changed with relative humidity showing a decrease of potential (i.e., increasingly negative) up to completion of the monolayer, followed by an increase (positive) after the first layer [77], as expected from the average upright orientation of the water dipole. The authors found also that when growing multilayer films at temperatures below 0 °C, the potential of the thickening film become highly negative, as shown in Fig. 11. These multilayer films however were metastable. This led to a model where ice on mica grows, at least for a few layers, with a ferroelectric structure with the O end up in the second and successive layers. The large accumulation of electrostatic energy made these multilayer films unstable and transformed abruptly into disordered films, with only the top layer exposing dangling H bonds.

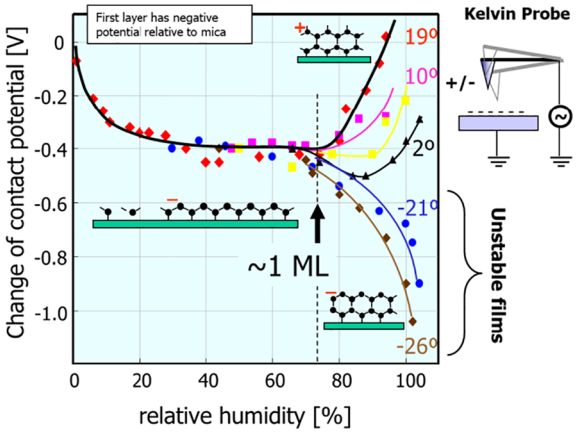

Fig. 11. Contact potential of a mica surface vs relative humidity (RH). At room-temperature (RT) the potential decreases until completion of the first layer and increases again above 80% RH, when second and higher layers form. Below 0 °C however, the potential becomes more negative above 80% RH. Above 100% RH the film grows rapidly and the potential reaching values of to −50 V in some areas. These very negative surfaces were unstable and the potential suddenly reversed to a positive value. The insets are schematic representations of the proposed water structures at different RHs and temperatures. Adapted from Ref. [77], with permission.

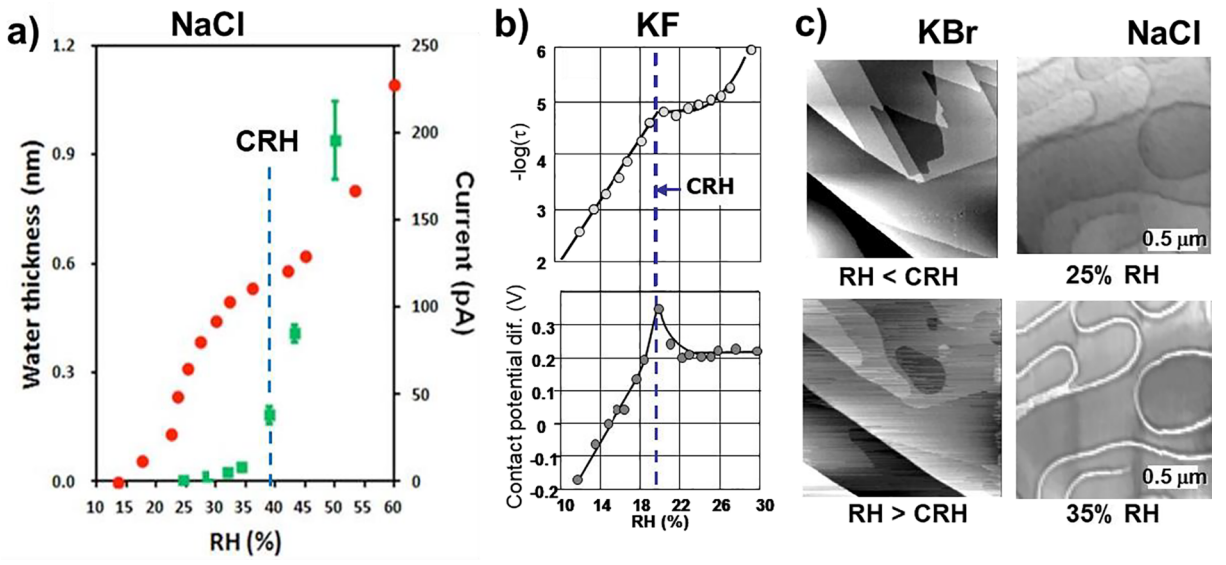

Fig.12. (a) Thickness of water layer on NaCl as a function of relative humidity (RH) calculated from the measured snap-in distance of the AFM probe. As the water thickness reaches 1–2 monolayer thickness, the surface conductivity increases dramatically at a Critical Relative Humidity value (CRH) characteristic of each alkali halide crystal. (b) Semilog plot of the time constant τ for solvated ion motion on a potassium fluoride cleaved surface exposed to increased RH, and simultaneously measured contact potential. Similar behavior was found in other alkali halide surfaces. (c) Left: Contact mode AFM images of KBr at low (top) and high humidity (bottom) relative to the CRH. Right: SPFM images of NaCl, as RH approaches CRH (40%) preferential solvation at steps is observed as an increase of intensity at the steps due to the higher polarizability of the surface. (Adapted with permission from [84,87]).

4.2. Water on salts

The adsorption of water on the cleavage face of various alkali halides (NaCl, KCl, KBr, KI) has been also studied as a function of humidity. It was found that a characteristic relative humidity value (CRH) exists that separates two water adsorption regimes identified by their strong differences in surface ionic conductivity [78,79] (Fig. 12a). On NaCl(1 0 0) adsorption isotherms calculated from infrared spectra [80,81] or from capillary condensation on an AFM probe, indicate that the first regime (RH < CRH) corresponds to a water coverage between zero and one or two monolayers (Fig. 12a).

Using SPFM [75,82–83] the role of water in modifying the polarizability and contact potential of alkali halides was studied. Below the CRH, where the surface conductivity is low, water adsorbs primarily at the steps [84] causing solvation of some ions that remain localized in the vicinity of the step. For a humidity higher than the CRH, large-scale modifications of the step morphology are produced (Fig. 12b). Experiments were performed to study the changes in contact potential and response time of the solvated ions as a function of relative humidity. These studies show that when the humidity is increased above CRH (Fig. 12b) a substantial change in the rate of increase of ionic mobility and also of surface potential occurs [84]. Although many other AFM experiments have been performed to study the surface modifications and step movements occurring above CRH [85,86], few studies have been performed to study the initial stages of water adsorption, below the CRH. The measurements using SPFM show that even below the CRH there is an increase in the electrostatic polarization force near steps, as shown in Fig. 12b [87,88].

The increase of polarization is related to the mobility of solvated ions, which was measured by the frequency dependence of the electrostatic force between the tip and the surface (in the range of kHz) [88]. The contact potential below the CRH was found to be different on the steps compared to the terraces [88], a result explained by the formation of dipoles resulting from the preferential solvation of one type of ion. As the RH increases, the contact potential difference between steps and terraces decreases and disappears completely at CRH [89–91]. At this point irreversible changes in the solvated ion distribution take place and the surface does not return to its original structure when dried. A number of theoretical studies have been performed to investigate the adsorption of water on NaCl(1 0 0). DFT [92,93] and ab-initio MD [94] calculations show that for a coverage of one monolayer water adsorption is favored on top of the Na ions. The most favorable configuration being with the water molecular plane roughly parallel to the surface. Monte Carlo [95] and MD [96] simulations of water on NaCl(1 0 0) also show that water molecules bind to the Na ions through the oxygen lone pair with similar configuration. Binding was found to be particularly strong at monoatomic step edges [86]. It was also found that below one monolayer, three-dimensional water clusters can form [94]. Simulations of the initial stages of dissolution of NaCl crystals determined a preferential initial dissolution of the Cl^- ion [97–99], which explains the evolution of the surface potential to more negative values as a function of humidity. As we discuss later, preferential adsorption at steps is not limited to alkali halides but it has been observed in other ionic crystals. In all cases water molecules solvate ions at the steps, showing some solvation preference for different ions. The type of ion that solvates first can depend on the history of water exposure and impurities in the crystal [89], nevertheless anions appear to solvate preferentially in the case of NaCl [88,97–98] and probably other salts. The

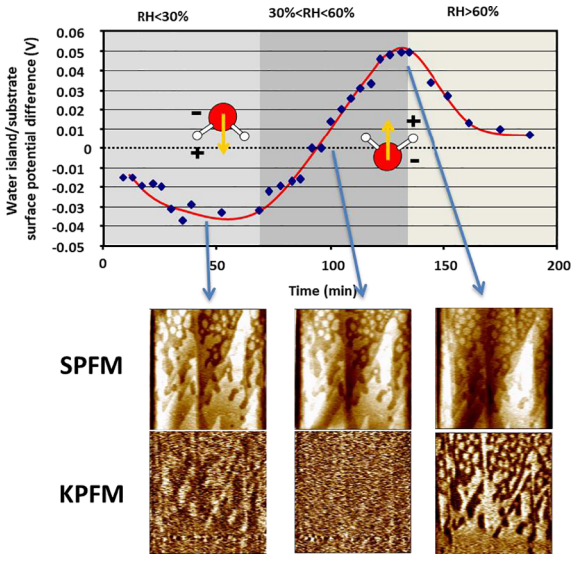

Fig. 13. Time evolution of the surface potential difference (SPD) between wet and dry regions as measured from KPFM images. Notice the sign crossover in the 30% < RH less than 60% region from −30 to +50 mV, indicating a flip of the water layer orientation. For RH > 60%, the contrast disappears with time. Solid line is just a guideline for the eye. Selected SPFM and KPFM 20 μm × 20 μm images are shown. At low RH some islands and some terraces completely covered by a water film can be observed. KPFM images show a contrast between with wet regions being darker (i.e., having a more negative surface potential) than dry regions. In the 30–60% RH region, the sign of the contrast between dry and wet regions continuously changes until it becomes brighter for the wet regions. (Adapted with permission form Verdaguer et al. [105]).

solvated anions move easily along the steps, producing a local negative potential relative to the terraces. The increased ionic mobility along steps can be detected through the increase of electrostatic force in the steps (Fig. 12c). At the CRH and at higher humidity, both cations and anions solvate at similar rates, removing the imbalance in the sign of mobile charges and triggering a large-scale motion of the steps that eliminates the contact potential difference between steps and terraces present at low humidity.

There has been a particular interest in the study of water adsorption on surfaces that have crystal structures with a lattice parameter close to that of the hexagonal faces of ice (I_h), because it is thought that those surfaces can induce ice nucleation. Among the different ionic crystals, one well-studied surface is the (1 1 1) face of BaF_2 [100]. The authors observed that at 30% RH water structures grew by island nucleation. They also found that the islands showed a height of about 5 Å for all substrates, which is indicative of the adsorption of two layers of water. From measurements of the time-dependent evolution of the film growth, the authors concluded that growth proceeds via island coalescence. A similar height was measured on BaF_2(1 1 1) by Santos et al. using a dynamic AFM method in which no direct mechanical interaction between the AFM probe and the water film occurs during imaging [101]. At high humidity (around 70% RH) Miura et al. [100] found that small islands with a height of about 1 nm and diameter of about 20 nm were initially formed, which then coalesced until a uniform water layer was created. In a macroscopic picture, the low aspect ratio of the initial islands would correspond to a small contact angle. The authors suggested that such a small contact angle indicates that droplets grow on top of a film of the same liquid. Below 50% RH droplets were not observed, suggesting the presence of only a monolayer or submonolayer of water. This is in line with the findings of Verdaguer et al. [102] where water films on BaF_2(1 1 1) were "trapped" by a graphene layer transferred to the surface at different humidity and then imaged using contact AFM mode (Fig. 13). Sadtchenko et al. [103,104] studied the adsorption of water and ice films on BaF_2(1 1 1) using infrared spectroscopy. The spectra were similar to those predicted theoretically for the surface bilayer of I_h ice, suggesting an ice-like hydrogen-bonded network even at room temperature. At multilayer coverage, the spectra became similar to that of bulk liquid water. The enthalpy of formation of the monolayer was found to be greater than that of condensation to either the liquid or solid phases. The absolute entropy of the monolayer revealed a high degree of order, with a value near that of ice at room temperature. Both enthalpy and entropy approached values for bulk liquid water at multilayer coverage. According to the authors, the results are consistent with an ice-like hexagonal water layer even at temperatures above the ice melting point, for monolayer coverage. Verdaguer et al. [105] used SPFM to study the evolution of surface potential contrast between dry and wet areas of a BaF_2(1 1 1) surface in the 20–50% RH range. Water was found to absorb forming islands, in agreement with previous results by Muira et al. [100]. The surface potential contrast between water islands and the bare substrate surface exhibited a sign crossover from negative (−30 mV) at low RHs to positive (+50 mV) at higher RHs, evidencing a cooperative and irreversible flipping of the average orientation of water dipoles, from pointing toward the surface to one in the opposite direction (see Fig. 13). None of the measured surface potential values was found to be compatible with an I_h bilayer or bulk liquid indicative of a high ordered solid-like monolayer different from I_h at low coverage. Monte Carlo simulations [106] of water adsorption on BaF_2(1 1 1) indicate that no ice-like bilayer forms for a coverage of one or more layers. The authors found that monomers adsorb preferentially with the hydrogen atoms pointing towards the surface. The energy penalty required to change this configuration to one more favorable for accommodating additional molecules and form hexagonal I_h bilayers is less than the energy gained with the formation of the increased hydrogen-bonding of I_h ice. The authors observed instead

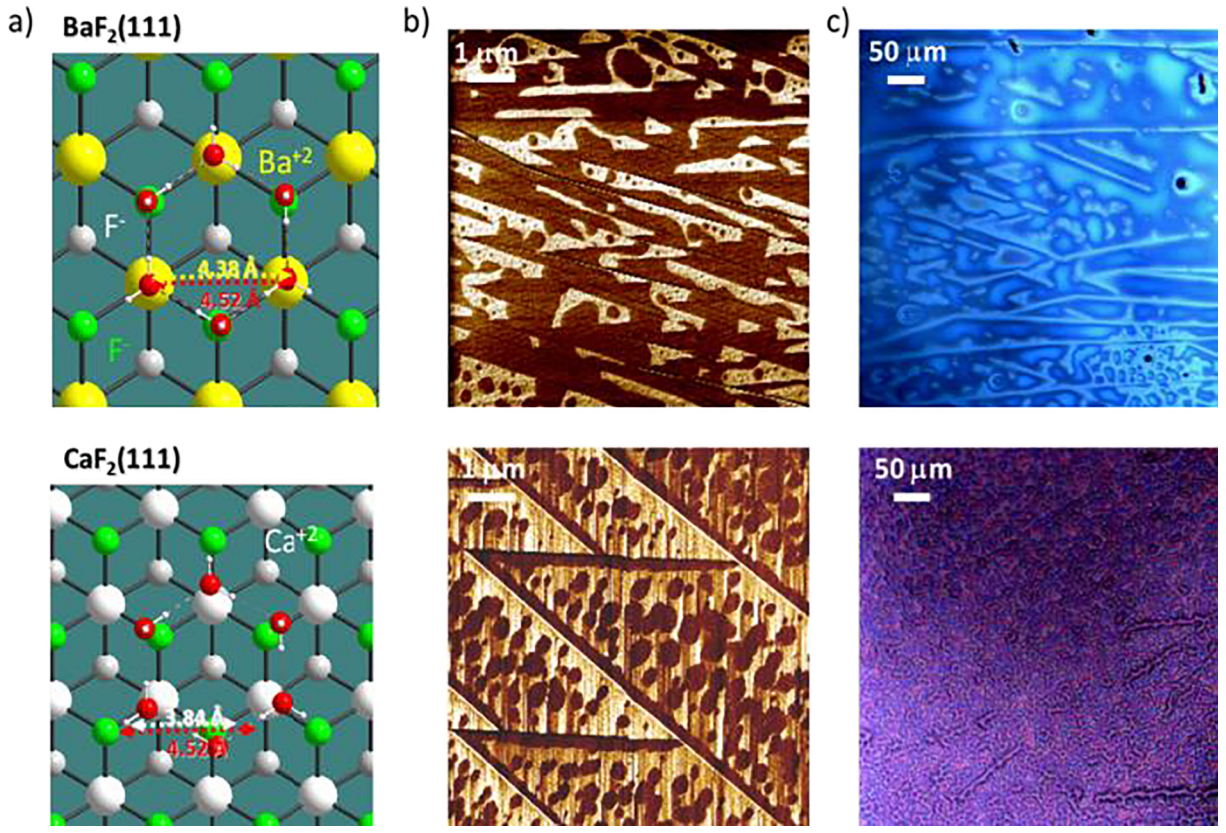

Fig. 14. (a) Schematic of hexagonal ice hexamer on a (1 1 1) BaF_2 and CaF_2 surface. Barium, calcium, upper fluorine, lower fluorine, oxygen and hydrogen atoms are represented by yellow, cyan, light gray, gray, red and white balls, respectively. The distances between the three water molecules forming the lower part of the bilayer structure almost match the distances between Ba ions in BaF_2 enabling pseudo-heteroepitaxy. However, on CaF_2 the difference is too large to accommodate a hexamer on the surface. (b) AFM phase contrast images showing water patches (darker in the images) absorbed on BaF_2(1 1 1) and CaF_2(1 1 1) under ambient conditions. c) Water adsorption on BaF_2(1 1 1) and CaF_2(1 1 1) observed by optical microscopy. The films on BaF_2 show polyhedral edges revealing the surface step structure while on CaF_2 small round droplets are formed that coalesce with increasing coverage. (Adapted with permission form Cardellach et al. [111]). (For interpretation of the references to color in this figure legend, the reader is referred to the web version of this article.)

cross-linked chains as the most favorable structure. It appears then that in order to be an effective ice nucleating substrate it is not enough to have a lattice constant close to that of ice, but that the orientation of the adsorbed water molecules must also be close to that in the tetrahedral ice structure [107]. This could explain why the formation of thicker ice films was found to be unstable even at −65 °C. After a few minutes, these thicker ice films spontaneously reassembled into an array of crystallites. Other infrared studies of ice on BaF_2(1 1 1) indicate that surface defects (pitting of the crystal), dramatically improves ice formation on the surface, probably by allowing adsorption of molecules in less restricted configurations [108].

DFT calculations have shown that at room temperature water molecules on BaF_2(1 1 1) surfaces are extremely mobile, forming a two-dimensional gas, and that they are only strongly bound at neutral vacancies [109]. SPFM images showed water accumulation at step edges with isolated islands on terraces that form two-dimensional bilayered structures [110]. Water accumulation seems to depend on step crystallography with steps with higher density of kinks surprisingly accumulating less water. The authors conclude that morphological defects are crucial for improving monolayer wetting and stabilization of multilayers on surfaces with good lattice match with hexagonal ice. This was observed also in optical microscopy experiments [111].

Even if close commensurability with the basal plane of I_h is not enough to induce growth of I_h on BaF_2(1 1 1) it still has an impact on the structure of adsorbed water films. Water films were compared with films formed on CaF_2(1 1 1), an isostructural crystal but with a surface lattice parameter smaller than BaF_2(1 1 1) [111]. Migration barriers for BaF_2 were found to be smaller than CaF_2 although the difference (0.3 eV for CaF_2 and 0.2 eV BaF_2) is not dramatic and similar mobility is expected at room temperature [109]. In spite of that such surfaces exhibit contrasting behaviors for both materials as shown in Fig. 14: while on BaF_2(1 1 1) two-dimensional water layers are formed after accumulation at step edges, CaF_2(1 1 1) does not promote the formation of such layers and only ribbons decorating the steps and water patches on terraces are observed. Optical microscope images reveal that this behavior also determines the way surfaces become wetted at a macroscopic level.

5. The liquid water-solid interface

In this final section, we review recent efforts to study the structure of solid interfaces with bulk liquid, and in the presence of electric fields. The knowledge of the structure and properties of such interfaces is key for a fundamental understanding and for the improvement of electrochemical processes, in electrocatalysis, photocatalysis, batteries and supercapacitors, to name a few. The interface region, typically a few nanometers thick, is known as the electrical double layer (EDL) and Helmholtz layer [112]. It contains solvent molecules and solvated ions in concentrations that depend on the strength of the electric field and on the electrolyte molarity [113]. These species interact by means of electrostatic, van der Walls forces, covalent and hydrogen bonding [114]. The strong electric field near the electrode surface can strongly modify the structure of water in aqueous electrolytes, which in the bulk is determined by H-bonding interactions and solvation. It can for example influence the orientation and electronic structure of the species close to the interface.

The scarcity of surface sensitive and element specific characterization techniques hinders the study of the atomic level mechanisms involved in the formation and structure of the electrical double layer [115]. Until now, mostly Infrared (IR), Raman and sum frequency generation (SFG) spectroscopies [116–118] have been used in the characterization of EDL. While these optical techniques provide invaluable information, they are not element specific and do not provide direct electronic structure information. The element-specific surface sensitive techniques, such as X-ray photoelectron spectroscopy (XPS), absorption and emission spectroscopies (XAS, XES) are in principle capable of addressing this problem. However, electron spectroscopy techniques usually require high vacuum for their operation and are not compatible with liquid environments and/or buried electrodes. These experimental hurdles have been overcome recently through several instrumental innovations [119–121].

X-ray absorption spectroscopy (XAS) in particular is an element-specific technique that can provide information on the electronic and geometric structure of molecules, and for that reason it has been extensively used to investigate the electronic structure of water using the oxygen K-edge [122–124]. Most investigations are typically performed collecting the photons generated by the decay of the core holes created by absorption of the X-rays, a method called fluorescence yield XAS (FY-XAS) [125–129]. Because of the micrometer penetration range of soft X-rays in condensed matter, the FY-XAS mode is essentially a bulk-sensitive technique. On the other hand, the core hole can also decay by emission of Auger electrons. These electrons, together with the secondary electrons generated in their path, can be detected in the so-called electron yield XAS mode (EY-XAS). The short inelastic mean free path of electrons, in the nanometer range, makes this mode surface sensitive and opens the possibility to make XAS a useful technique for electrode-electrolyte interface studies in liquid environments by simply detecting the current at the electrode due to emission imbalance at the liquid interface. Problems present in electrochemical environments, such as ionic currents from electrochemical processes that can be orders of magnitude higher than the EY-XAS signal, were recently circumvented by the introduction of modulation of the X-ray beam intensity which generates an AC signal component in the EY-XAS. This signal can be selectively filtered with lock-in amplifiers [130]. Other methods to study solid-liquid interfaces have been developed, for example using electron transparent membranes based in graphene [131,132].

Here we report recent progress using the EY-XAS with X-ray intensity modulation and lock-in detection to determine the electronic structure and orientation of water molecules near a gold electrode as a function of the applied potential. The gold electrode, in the form of a 20 nm polycrystalline thin film, was vapor deposited onto a 100 nm thin SiN_x membrane [130], which closes an electrochemical cell separating the electrolyte phase from the vacuum chamber of the Synchrotron beamline. The gold film on the inside part of the membrane was the working electrode in contact with a 10 μM aqueous solution of NaCl. A schematic of the electrochemical cell and AC modulation scheme detection is shown in Fig. 15(i) and (ii).

The O K-edge spectra of water near the Au electrode under open circuit voltage (OCV) are shown in Fig. 15(iii). Fig. 15(iv) shows a snap-shot of the ab-initio molecular dynamics simulation of water from which the XAS spectra were calculated. The feature around 535 eV [123,124,133] which is observed in the FY-XAS of Fig. 15(iii) curve (a), is due to the approximately 20% fraction of bulk water molecules with dangling hydrogen bonds [134]. This feature is suppressed in the surface sensitive measurement EY-XAS spectrum shown in curve (b). When the Au electrode was functionalized with C_{16}-thiols the pre-peak at 535 eV in EY-XAS curve (c) was present again, indicating no interaction between Au and water. First principle calculations explained the suppression of the peak of water in contact with Au as a combination of water orientation (for molecules pointing the O to the gold, or parallel to the surface), and by delocalization of its LUMO orbitals due to hybridization with Au orbital when the H points towards the electrode.

The EY-XAS spectra collected as a function of applied potential are shown in Fig. 16a. When the electrode is negatively biased, the 535 eV peak is present as a result of the increase in the number of molecules with dangling H bonds, some pointing to the substrate and some parallel, as shown in Fig. 16c. When the Au surface is in OCP or positively polarized the pre-peak at around 535 eV is suppressed because the positively charged surface favors more water molecules with O atoms pointing to the Au electrode. As shown in Fig. 16b, the spectra derived from ab-initio molecular dynamics simulations and calculated XAS spectra fit well the experimental ones [130]. From the fit, the distribution of water species with different orientations and H-bonding structures shown in Fig. 16c was obtained. An enhanced double donor (DD) population at positive bias is obtained, while at negative bias the change in the orientation of the water molecules greatly disrupts the hydrogen bonding, leading to a 25% increase in the population of the single donors parallel to the surface ($SD^{||}$) and thus enhancing the pre-edge.

Because the investigation of solid-liquid interfaces is of crucial importance in applications including energy storage and conversions systems, a number of novel *operando* methods are being developed in addition to the EY-XAS based on membranes sealing the liquid cell described above. Several recent promising approaches are based on the use of photo-electron spectroscopy (XPS) through a liquid film around the sample electrode. The short mean free path of photoelectrons limits the thickness of this liquid film to a few nanometers depending on the kinetic energy. In order to accomplish these measurements, two possibilities are being

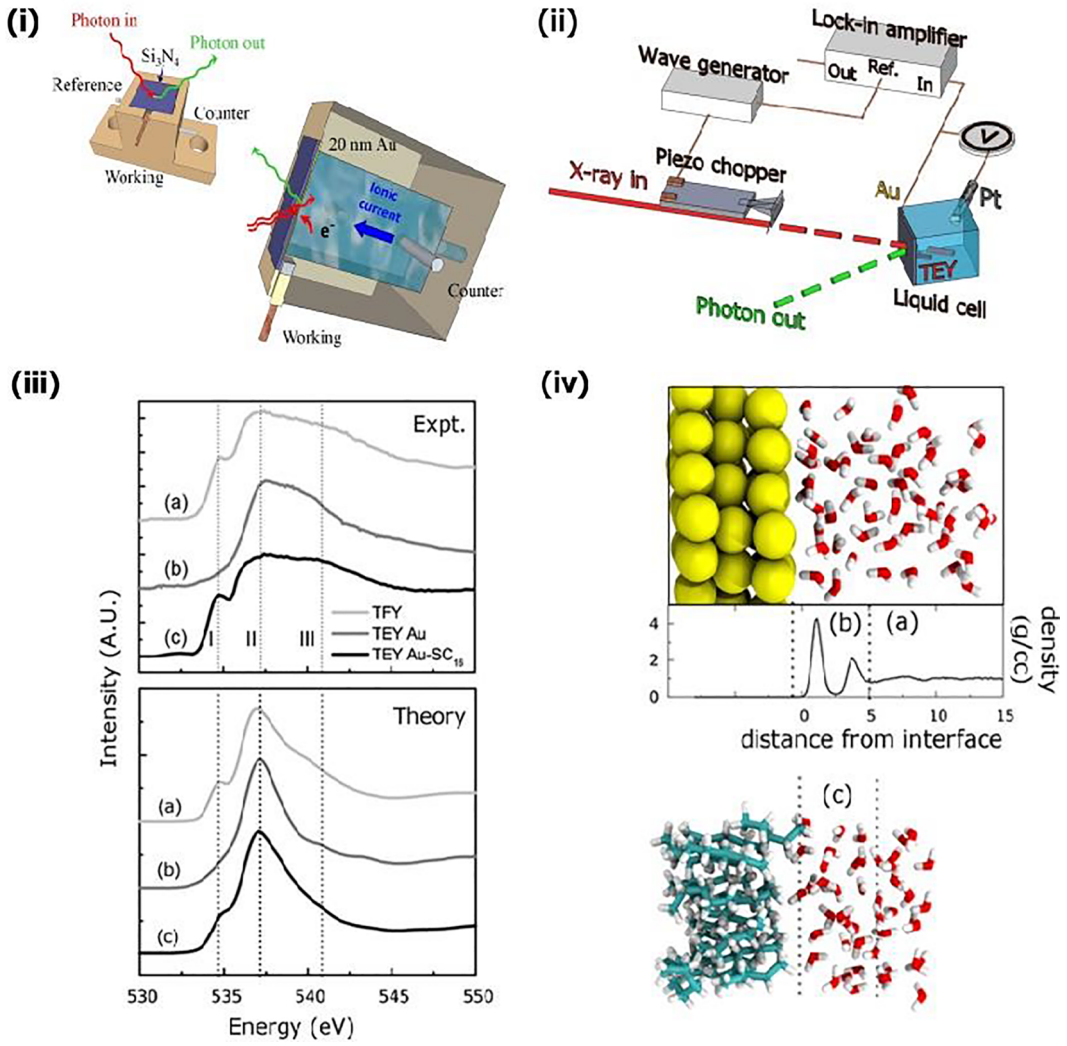

Fig. 15. (i) Schematic of the electrochemical cell composed of a Si_3N_4 membrane (~100 nm thick) that separates the liquid volume from the vacuum outside. A 20 nm thick gold electrode was deposited on the back side of the membrane in contact with the electrolyte. X-rays from the synchrotron traverse the SiN and Au films are absorbed by the O atoms of water. The decay of the core-hole produces a fluorescent X-ray emission and also electrons, both signals are proportional to the absorption cross-section. In the method employed here, the electron emission current was collected at the gold electrode. In this way, and due to the short mean free path of electrons (~1 nm), only a few layers of water next to the Au electrode contribute to the XAS signal, while the fluorescence X-rays collected outside the cell report the XAS signal from bulk water. (ii) AC modulation scheme of the incoming X-ray and selective frequency detection with a lock-in amplifier. (iii) Experimental (top) and calculated (bottom) O K-edge spectra of water measured with the lock-in technique under open circuit voltage (OCV) conditions: Curve (a) corresponds to the bulk sensitive fluorescence yield (TFY).; curve (b) to the total electron yield (TEY); curve (c) corresponds to the TEY of water after covering the gold surface with a hexadecanethiol monolayer. (iv) Ab-initio Molecular dynamic simulation of the water structure near the gold electrode. Adapted with permission from [130]. The calculated water structure from ab-initio Molecular dynamic simulations is shown in (iv) along with the mass density profile.

explored. One is through a thin film of liquid forming a meniscus held by capillary forces, the so-called “dip & pull” method [135]. Combined with X-ray of higher energy, the method has been demonstrated to work for relevant electrochemical processes such as the structure of the electrical double layer [113] and electro/photo-catalytic processes [136]. Combining the meniscus method with the standing wave technique [137] it should be possible to provide highly detailed information across liquid/solid interfaces with sub-nanometer resolution. Yet another technique is explored that entails the use of ultra-thin graphene membranes to separate the liquid phase from the vacuum side where the analyzer is placed [132], which can be used with soft X-rays. Using this approach, it is possible to investigate relevant electrochemical processes [131] as well as confine liquid between a substrate and a graphene layer [138]. This approach together with new upcoming developments in the photon-sources and detection techniques will enable the investigation of electrified solid-liquid interfaces that remain elusive with the current state of the art methods.

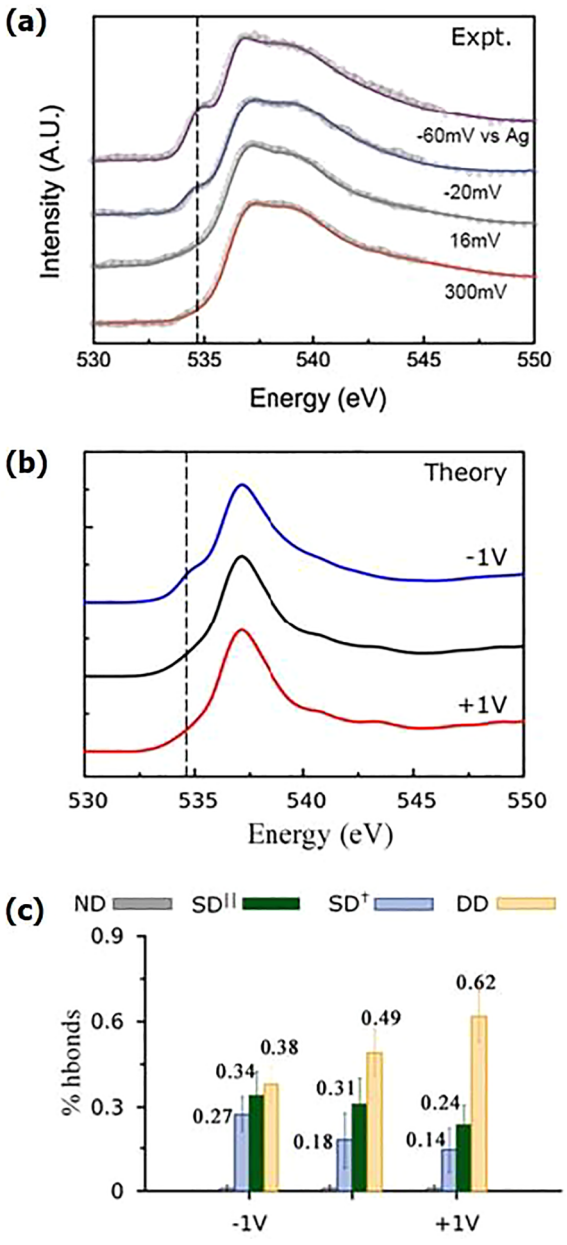

Fig. 16. (a) O K-edge EY-XAS measurements of water collected at the Au electrode under different potentials, versus Ag quasi-reference electrode. (b) Calculated spectra. (c) Population of hydrogen bonded water molecules, with color bars for various orientations and H-bonding conditions. (Adapted with permission from [130]).

Acknowledgments

This work was supported by the Office of Basic Energy Sciences (BES), Division of Materials Sciences and Engineering, of the U.S. Department of Energy (DOE) under Contract No. DE-AC02-05CH11231, through the Structure and Dynamics of Materials Interfaces program (FWP KC31SM). S.M. acknowledges funding from the by the German Science Foundation (DFG) through the Cluster of Excellence EXC 315 “Engineering of Advanced Materials” and as the European Research Council (ERC-2014-StG SURFLINK No. 637831). A.V. acknowledges funding from projects MAT2016-77852-C2-1-R and SEV-2015-0496, MINECO, Spain.

References

[1] P.A. Thiel, T.E. Madey, The interaction of water with solid surfaces: fundamental aspects, Surf. Sci. Rep. 7 (1987) 211–385.
[2] M.A. Henderson, The interaction of water with solid surfaces: fundamental aspects revisited, Surf. Sci. Rep. 46 (2002) 1–308.

[3] A. Hodgson, S. Haq, Water adsorption and the wetting of metal surfaces, Surf. Sci. Rep. 64 (2009) 381–451.
[4] L.J. Lauhon, W. Ho, Inducing and observing the abstraction of a single hydrogen atom in bimolecular reactions with a scanning tunneling microscope, J. Phys. Chem. B. 105 (2001) 3987–3992.
[5] K. Morgenstern, J. Nieminen, Intermolecular bond length of ice on Ag(111), Phys. Rev. Lett. 88 (2002) 66102.
[6] K. Morgenstern, Scanning tunnelling microscopy investigation of water in submonolayer coverage on Ag(111), Surf. Sci. 504 (2002) 293–300.
[7] K. Morgenstern, K.-H. Rieder, Formation of the cyclic ice hexamer via excitation of vibrational molecular modes by the scanning tunneling microscope, J. Chem. Phys. 116 (2002) 5746–5752.
[8] K. Morgenstern, K.-H. Rieder, Dissociation of water molecules with the scanning tunnelling microscope, Chem. Phys. Lett. 358 (2002) 250–256.
[9] K. Morgenstern, J. Nieminen, Imaging water on Ag(111): Field induced reorientation and contrast inversion, J. Chem. Phys. 120 (2004) 10786–10791.
[10] A. Michaelides, K. Morgenstern, Ice nanoclusters at hydrophobic metal surfaces, Nat. Mater. 6 (2007) 597–601.
[11] T. Komeda, H. Fukidome, Y. Kim, M. Kawai, Scanning tunneling microscopy study of water molecules on Pd(110) at cryogenic temperature, Jpn. J. Appl. Phys. 41 (2002) 4932–4935.
[12] E. Fomin, M. Tatarkhanov, T. Mitsui, M. Rose, D.F. Ogletree, M. Salmeron, Vibrationally assisted diffusion of H_2O and D_2O on Pd(111), Surf. Sci. 600 (2006) 542–546.
[13] T.K. Shimizu, A. Mugarza, J.I. Cerdá, M. Heyde, Y. Qi, U.D. Schwarz, D.F. Ogletree, M. Salmeron, Surface species formed by the adsorption and dissociation of water molecules on a Ru(0001) surface containing a small coverage of carbon atoms studied by scanning tunneling microscopy, J. Phys. Chem. C. 112 (2008) 7445–7454.
[14] A. Michaelides, V.A. Ranea, P.L. de Andres, D.A. King, General model for water monomer adsorption on close-packed transition and noble metal surfaces, Phys. Rev. Lett. 90 (2003) 216102.
[15] K. Morgenstern, H. Gawronski, M. Mehlhorn, K.-H. Rieder, Local investigation of electron-induced processes in water-metal systems, J. Mod. Opt. 10 (2004) 2813–2819.
[16] L. Árnadóttir, E.M. Stuve, H. Jónsson, Adsorption of water monomer and clusters on platinum(111) terrace and related steps and kinks I. Configurations, energies, and hydrogen bonding, Surf. Sci. 604 (2010) 1978–1986.
[17] K. Motobayashi, L. Árnadóttir, C. Matsumoto, E.M. Stuve, H. Jónsson, Y. Kim, M. Kawai, Adsorption of water dimer on platinum(111): identification of the –OH Pt hydrogen bond, ACS Nano 8 (2014) 11583–11590.
[18] K. Motobayashi, C. Matsumoto, Y. Kim, M. Kawai, Vibrational study of water dimers on Pt(1 1 1) using a scanning tunneling microscope, Surf. Sci. 602 (2008) 3136–3139.
[19] A. Mugarza, T.K. Shimizu, D.F. Ogletree, M. Salmeron, Chemical reactions of water molecules on Ru(0001) induced by selective excitation of vibrational modes, Surf. Sci. 603 (2009) 2030–2036.
[20] T. Mitsui, M.K. Rose, E. Fomin, D.F. Ogletree, M. Salmeron, Water diffusion and clustering on Pd(111), Science 297 (2002) 1850–1852.
[21] V.A. Ranea, A. Michaelides, R. Ramírez, P.L. De Andres, J.A. Vergés, D.A. King, Water dimer diffusion on Pd{111} assisted by an H-bond donor-acceptor tunneling exchange, Phys. Rev. Lett. 92 (2004) 136104.
[22] L. Árnadóttir, E.M. Stuve, H. Jónsson, Adsorption of water monomer and clusters on platinum(111) terrace and related steps and kinks II. Surface diffusion, Surf. Sci. 606 (2012) 233–238.
[23] T. Kumagai, M. Kaizu, H. Okuyama, S. Hatta, T. Aruga, I. Hamada, Y. Morikawa, Tunneling dynamics of a hydroxyl group adsorbed on Cu(110), Phys. Rev. B 79 (2009) 035423.
[24] H.-J. Shin, J. Jung, K. Motobayashi, S. Yanagisawa, Y. Morikawa, Y. Kim, M. Kawai, State-selective dissociation of a single water molecule on an ultrathin MgO film, Nat. Mater. 9 (2010) 442–447.
[25] J. Cerda, A. Michaelides, M.L. Bocquet, P.J. Feibelman, T. Mitsui, M. Rose, E. Fomin, M. Salmeron, Novel water overlayer growth on Pd(111) characterized with scanning tunneling microscopy and density functional theory, Phys. Rev. Lett. 93 (2004) 116101.
[26] S. Meng, E.G. Wang, S.W. Gao, Water adsorption on metal surfaces: a general picture from density functional theory studies, Phys. Rev. B 69 (2004) 195404.
[27] M. Tatarkhanov, D.F. Ogletree, F. Rose, T. Mitsui, E. Fomin, S. Maier, M. Rose, J.I. Cerdá, M. Salmeron, Metal- and Hydrogen-bonding competition during water adsorption on Pd(111) and Ru(0001), J. Am. Chem. Soc. 131 (2009) 18425–18434.
[28] S. Maier, I. Stass, J.I. Cerdá, M. Salmeron, Unveiling the mechanism of water partial dissociation on Ru(0001), Phys. Rev. Lett. 112 (2014).
[29] S. Maier, I. Stass, T. Mitsui, P.J. Feibelman, K. Thürmer, M. Salmeron, Adsorbed water-molecule hexagons with unexpected rotations in islands on Ru(0001) and Pd(111), Phys. Rev. B 85 (2012) 155434.
[30] S. Nie, P.J. Feibelman, N.C. Bartelt, K. Thürmer, Pentagons and heptagons in the first water layer on Pt(111), Phys. Rev. Lett. 105 (2010) 026102.
[31] K. Thürmer, S. Nie, P.J. Feibelman, N.C. Bartelt, Clusters, molecular layers, and 3D crystals of water on Ni(111), J. Chem. Phys. 141 (2014) 18C520.
[32] D.L. Doering, T.E. Madey, The adsorption of water on clean and oxygen-dosed Ru(001), Surf. Sci. 123 (1982) 305–337.
[33] P.J. Feibelman, Partial dissociation of water on Ru(0001), Science 295 (2002) 99–102.
[34] F. McBride, G.R. Darling, K. Pussi, A. Hodgson, Tailoring the structure of water at a metal surface: a structural analysis of the water bilayer formed on an alloy template, Phys. Rev. Lett. 106 (2011) 226101.
[35] J. Carrasco, A. Michaelides, M. Forster, S. Haq, R. Raval, A. Hodgson, A one-dimensional ice structure built from pentagons, Nat. Mater. 8 (2009) 427–431.
[36] A. Shiotari, Y. Sugimoto, Ultrahigh-resolution imaging of water networks by atomic force microscopy, Nat. Commun. 8 (2017) 14313.
[37] T. Yamada, S. Tamamori, H. Okuyama, T. Aruga, Anisotropic water chain growth on Cu(110) observed with scanning tunneling microscopy, Phys. Rev. Lett. 96 (2006) 036105.
[38] K. Andersson, A. Nikitin, L.G.M. Pettersson, A. Nilsson, H. Ogasawara, Water dissociation on Ru(001): an activated process, Phys. Rev. Lett. 93 (2004) 196101.
[39] A. Michaelides, A. Alavi, D.A. King, Different surface chemistries of water on Ru(0001): from monomer adsorption to partially dissociated bilayers, J. Am. Chem. Soc. 125 (2003) 2746–2755.
[40] J. Weissenrieder, A. Mikkelsen, J.N. Andersen, P.J. Feibelman, G. Held, Experimental evidence for a partially dissociated water bilayer on Ru(0001), Phys. Rev. Lett. 93 (2004) 196102.
[41] M. Tatarkhanov, E. Fomin, M. Salmeron, K. Andersson, H. Ogasawara, L.G.M. Pettersson, A. Nilsson, J.I. Cerda, The structure of mixed H_2O-OH monolayer films on Ru(0001), J. Chem. Phys. 129 (2008) 154109.
[42] N.S. Faradzhev, K.L. Kostov, P. Feulner, T.E. Madey, D. Menzel, Stability of water monolayers on Ru(0001): thermal and electronically induced dissociation, Chem. Phys. Lett. 415 (2005) 165–171.
[43] C. Clay, S. Haq, A. Hodgson, Intact and dissociative adsorption of water on Ru(0001), Chem. Phys. Lett. 388 (2004) 89–93.
[44] A. Shavorskiy, M.J. Gladys, G. Held, Chemical composition and reactivity of water on hexagonal Pt-group metal surfaces, Phys. Chem. Chem. Phys. 10 (2008) 6150–6159.
[45] C. Badan, Y. Heyrich, M.T.M. Koper, L.B.F. Juurlink, Surface structure dependence in desorption and crystallization of thin interfacial water films on platinum, J. Phys. Chem. Lett. 7 (2016) 1682–1685.
[46] D. Donadio, L.M. Ghiringhelli, L. Delle Site, Autocatalytic and cooperatively stabilized dissociation of water on a stepped platinum surface, J. Am. Chem. Soc. 134 (2012) 19217–19222.
[47] M.J. Kolb, F. Calle-Vallejo, L.B.F. Juurlink, M.T.M. Koper, Density functional theory study of adsorption of H_2O, H, O, and OH on stepped platinum surfaces, J. Chem. Phys. 140 (2014) 134708.
[48] G.B. Fisher, B.A. Sexton, Identification of an adsorbed hydroxyl species on the Pt(111) surface, Phys. Rev. Lett. 44 (1980) 683–686.
[49] C. Clay, S. Haq, A. Hodgson, Hydrogen bonding in mixed OH + H_2O overlayers on Pt(111), Phys. Rev. Lett. 92 (2004) 046102.
[50] M.J. Gladys, A.A. El-Zein, A. Mikkelsen, J.N. Anderson, G. Held, Modifying the adsorption characteristics of water on Ru(0001) with preadsorbed oxygen, Phys. Rev. B 78 (2008) 035409.
[51] M.J. Gladys, A. Mikkelsen, J.N. Andersen, G. Held, Water adsorption on O-covered Ru(0001): coverage-dependent change from dissociation to molecular

adsorption, Chem. Phys. Lett. 414 (2005) 311–315.
[52] P. Cabrera-Sanfelix, D. Sanchez-Portal, A. Mugarza, T.K. Shimizu, M. Salmeron, A. Arnau, Water adsorption on O(2×2)/Ru(0001): STM experiments and first-principles calculations, Phys. Rev. B 76 (2007) 205438.
[53] A. Mugarza, T.K. Shimizu, P. Cabrera-Sanfelix, D. Sanchez-Portal, A. Arnau, M. Salmeron, Adsorption of water on O(2×2)/Ru(0001): thermal stability and inhibition of dissociation, J. Phys. Chem. C 112 (2008) 14052–14057.
[54] S. Maier, P. Cabrera-Sanfelix, I. Stass, D. Sanchez-Portal, A. Arnau, M. Salmeron, Water-induced surface reconstruction of oxygen (2×1) covered Ru(0001), Phys. Rev. B 82 (2010) 075421.
[55] B. A. Lechner, Y. Kim, P.J. Feibelman, G. Henkelman, H. Kang, M. Salmeron, Solvation and reaction of ammonia in molecularly thin water films, J. Phys. Chem. C 119 (40) (2015) 23052–23058.
[56] H. Ogasawara, B. Brena, D. Nordlund, M. Nyberg, A. Pelmenschikov, L.G.M. Pettersson, A. Nilsson, Structure and bonding of water on Pt(111), Phys. Rev. Lett. 89 (2002) 276102.
[57] Greg A. Kimmel, Nikolay G. Petrik, Zdenek Dohnálek, Bruce D. Kay, Crystalline ice growth on Pt(111): observation of a hydrophobic water monolayer, Phys. Rev. Lett. 95 (2005) 166102.
[58] Greg A. Kimmel, Nikolay G. Petrik, Zdenek Dohnálek, Bruce D. Kay, Layer-by-layer growth of thin amorphous solid water films on Pt(111) and Pd(111), J. Chem. Phys. 125 (2006) 044713.
[59] S. Maier, B.A.J. Lechner, G.A. Somorjai, M. Salmeron, Growth and structure of the first layers of ice on Ru(0001) and Pt(111), J. Am. Chem. Soc. 138 (2016) 3145–3151.
[60] K. Thürmer, N.C. Bartelt, Growth of multilayer ice films and the formation of cubic ice imaged with STM, Phys. Rev. B 77 (2008) 195425.
[61] K. Thürmer, N.C. Bartelt, Nucleation-limited dewetting of ice films on Pt(111), Phys. Rev. Lett. 100 (2008) 186101.
[62] G. Zimbitas, S. Haq, A. Hodgson, The structure and crystallization of thin water films on Pt(111), J. Chem. Phys. 123 (2005) 174701–174709.
[63] K. Thürmer, S. Nie, Formation of hexagonal and cubic ice during low-temperature growth, Proc. National Acad. Sci. 110 (2013) 11757–11762.
[64] P. Pirzadeh, P.G. Kusalik, On understanding stacking fault formation in ice, J. Am. Chem. Soc. 133 (2011) 704–707.
[65] M. Mehlhorn, K. Morgenstern, Faceting during the transformation of amorphous to crystalline ice, Phys. Rev. Lett. 99 (2007) 246101.
[66] F.J. Giessibl, Advances in atomic force microscopy, Rev. Mod. Phys. 75 (2003) 949–983.
[67] J. Guo, X. Meng, J. Chen, J. Peng, J. Sheng, X.-Z. Li, L. Xu, J.-R. Shi, E. Wang, Y. Jiang, Real-space imaging of interfacial water with submolecular resolution, Nat. Mater. 13 (2014) 184–189.
[68] X. Meng, J. Guo, J. Peng, J. Chen, Z. Wang, J.-R. Shi, X.-Z. Li, E.-G. Wang, Y. Jiang, Direct visualization of converted proton tunnelling in a water nanocluster, Nat. Phys. 11 (2015) 235–239.
[69] J. Guo, J.-T. Lu, Y. Feng, J. Chen, J. Peng, Z. Lim, X. Meng, Z. Wang, X.-Z. Li, E.-G. Wang, Y. Jiang, Nuclear quantum effects of hydrogen bonds probed by tip-enhanced inelastic electron tunneling, Science 352 (2016) 321–325.
[70] S.-C. Heidorn, C. Bertram, P. Cabrera-Sanfelix, K. Morgenstern, Consecutive mechanism in the diffusion of D_2O on a NaCl(100) bilayer, ACS Nano 9 (2015) 3572–3578.
[71] R. Mu, Z. Zhao, Z. Dohnálek, J. Gong, Structural motifs of water on metal oxide surfaces, Chem. Soc. Rev. 46 (2017) 1785–1806.
[72] D. Halwidl, B. Stoger, W. Mayr-Schmolzer, J. Pavelec, D. Fobes, J. Peng, Z.Q. Mao, G.S. Parkinson, M. Schmid, F. Mittendorfer, J. Redinger, U. Diebold, Nat. Mater. 15 (2016) 450–456.
[73] A.L. Sumner, E.J. Menke, Y. Dubowski, J.T. Newberg, R.M. Penner, J.C. Hemminger, L.M. Wingen, T. Brauers, B.J. Finlayson-Pitts, The nature of water on surfaces of laboratory systems and implications for heterogeneous chemistry in the troposphere, Phys. Chem. Chem. Phys. 6 (2004) 604–613.
[74] S. Santos, A. Verdaguer, Imaging water thin films in ambient conditions using atomic force microscopy, Materials 9 (2016) 182.
[75] J. Hu, X.-D. Xiao, D.F. Ogletree, M. Salmeron, Imaging the condensation and evaporation of molecularly thin films of water with nanometer resolution, Science 268 (1995) 267–269.
[76] P.B. Miranda, L. Xu, Y.R. Shen, M. Salmeron, Ice-like water monolayer adsorbed on mica at room temperature, Phys. Rev. Lett. 81 (1998) 5876.
[77] H. Bluhm, T. Inoue, M. Salmeron, Formation of dipole-oriented water films on mica substrates at ambient conditions, Surf. Sci. 462 (2000) L599–L602.
[78] M. Hucher, A. Oberlin, R. Hocart, Adsorption of water vapour on cleavage surfaces of some alkali halides, B Soc. Fr. Mineral. Cr. 90 (1967) 320-&.
[79] L. Yang, J.F. He, Y. Shen, X.W. Li, J.L. Sun, D.M. Czajkowsky, Z.F. Shao, Nanoscopic characterization of the water vapor-salt interfacial layer reveals a unique biphasic adsorption process, Sci. Rep. 6 (2016) 31688.
[80] M.C. Foster, G.E. Ewing, Adsorption of water on the NaCl(001) surface. II. An infrared study at ambient temperatures, J. Chem. Phys. 112 (2000) 6817–6826.
[81] G.E. Ewing, Thin film water, J. Phys. Chem. B 108 (2004) 15953–15961.
[82] J. Hu, X.D. Xiao, M. Salmeron, Scanning polarization force microscopy – a technique for imaging liquids and weakly adsorbed layers, Appl. Phys. Lett. 67 (1995) 476–478.
[83] J. Hu, X.D. Xiao, D.F. Ogletree, M. Salmeron, The structure of molecularly thin films of water on mica in humid environments, Surf. Sci. 344 (1995) 221–236.
[84] M. Luna, F. Rieutord, N.A. Melman, Q. Dai, M. Salmeron, Adsorption of water on alkali halide surfaces studied by scanning polarization force microscopy, J. Phys. Chem. A 102 (1998) 6793–6800.
[85] H. Shindo, M. Ohashi, O. Tateishi, A. Seo, Atomic force microscopic observation of step movements on NaCl(001) and NaF(001) with the help of adsorbed water, J. Chem. Soc. Faraday T. 93 (1997) 1169–1174.
[86] S. Garcia-Manyes, A. Verdaguer, P. Gorostiza, F. Sanz, Alkali halide nanocrystal growth and etching studied by AFM and modeled by MD simulations, J. Chem. Phys. 120 (2004) 2963–2971.
[87] Q. Dai, J. Hu, M. Salmeron, Adsorption of water on NaCl(100) surfaces: role of atomic steps, J. Phys. Chem. B 101 (1997) 1994–1998.
[88] A. Verdaguer, G.M. Sacha, M. Luna, F.D. Ogletree, M. Salmeron, Initial stages of water adsorption on NaCl(100) studied by scanning polarization force microscopy, J. Chem. Phys 123 (2005) 124703.
[89] S. Ghosal, A. Verdaguer, J.C. Hemminger, M. Salmeron, In situ study of water-induced segregation of bromide in bromide-doped sodium chloride by scanning polarization force microscopy, J. Phys. Chem. A 109 (2005) 4744–4749.
[90] K. Arima, P. Jiang, D.S. Lin, A. Verdaguer, M. Salmeron, Ion segregation and deliquescence of alkali halide nanocrystals on SiO_2, J. Phys. Chem. A 113 (2009) 9715–9720.
[91] D.A. Bruzewicz, A. Checco, B.M. Ocko, E.R. Lewis, R.L. McGraw, S.E. Schwartz, Reversible uptake of water on NaCl nanoparticles at relative humidity below deliquescence point observed by noncontact environmental atomic force microscopy, J. Chem. Phys. 134 (2011) 044702.
[92] J.M. Park, J.H. Cho, K.S. Kim, Atomic structure and energetics of adsorbed water on the NaCl(001) surface, Phys. Rev. B 69 (2004) 233403.
[93] Y. Yang, S. Meng, E.G. Wang, Water adsorption on a NaCl(001) surface: a density functional theory study, Phys. Rev. B 74 (2006) 245409.
[94] H. Meyer, P. Entel, J. Hafner, Physisorption of water on salt surfaces, Surf. Sci. 488 (2001) 177–192.
[95] O. Engkvist, A.J. Stone, Adsorption of water on NaCl(001). I. Intermolecular potentials and low temperature structures, J. Chem. Phys. 110 (1999) 12089–12096.
[96] E. Stockelmann, E.M. Aydt, R. Hentschke, Simulation of adsorption isotherms of water on ionic surfaces, J. Mol. Model. 3 (1997) 347–354.
[97] L.M. Liu, A. Laio, A. Michaelides, Initial stages of salt crystal dissolution determined with ab initio molecular dynamics, Phys. Chem. Chem. Phys. 13 (2011) 13162–13166.
[98] P. Cabrera-Sanfelix, D.S. Portal, A. Verdaguer, G.R. Darling, M. Salmeron, A. Arnau, Spontaneous emergence of Cl- anions from NaCl(100) at low relative humidity, J. Phys. Chem. C 111 (2007) 8000–8004.
[99] A. Verdaguer, G.M. Sacha, H. Bluhm, M. Salmeron, Molecular structure of water at interfaces: wetting at the nanometer scale, Chem. Rev. 106 (2006) 1478–1510.
[100] K. Miura, T. Yamada, M. Ishikawa, S. Okita, Apparent contrast of molecularly thin films of water at ionic crystal surfaces, Appl. Surf. Sci. 140 (1999) 415–421.
[101] S. Santos, A. Verdaguer, T. Souier, N.H. Thomson, M. Chiesa, Measuring the true height of water films on surfaces, Nanotechnology 22 (2011) 46.

[102] A. Verdaguer, J.J. Segura, L. Lopez-Mir, G. Sauthier, J. Fraxedas, Communication: growing room temperature ice with graphene, J. Chem. Phys. 138 (2013) 121101.
[103] V. Sadtchenko, G.E. Ewing, Interfacial melting of thin ice films: an infrared study, J. Chem. Phys. 116 (2002) 4686–4697.
[104] V. Sadtchenko, G.E. Ewing, D.R. Nutt, A.J. Stone, Instability of ice films, Langmuir 18 (2002) 4632–4636.
[105] A. Verdaguer, M. Cardellach, J. Fraxedas, Thin water films grown at ambient conditions on BaF_2(111) studied by scanning polarization force microscopy, J. Chem. Phys. 2008 (129) (2008) 174705.
[106] D.R. Nutt, A.J. Stone, Adsorption of water on the BaF_2(111) surface, J. Chem. Phys. 117 (2002) 800–807.
[107] D.R. Nutt, A.J. Stone, Ice nucleation on a model hexagonal surface, Langmuir 20 (2004) 8715–8720.
[108] P. Conrad, G.E. Ewing, R.L. Karlinsey, V. Sadtchenko, Ice nucleation on BaF_2(111), J. Chem. Phys. 122 (2005) 064709.
[109] A.S. Foster, T. Trevethan, A.L. Shluger, Structure and diffusion of intrinsic defects, adsorbed hydrogen, and water molecules at the surface of alkali-earth fluorides calculated using density functional theory, Phys. Rev. B 80 (2009) 115421.
[110] M. Cardellach, A. Verdaguer, J. Santiso, J. Fraxedas, Two-dimensional wetting: The role of atomic steps on the nucleation of thin water films on BaF_2(111) at ambient conditions, J. Chem. Phys. 132 (2010) 234708.
[111] M. Cardellach, A. Verdaguer, J. Fraxedas, Defect-induced wetting on BaF_2(111) and CaF_2(111) at ambient conditions, Surf. Sci. 605 (2011) 1929–1933.
[112] A.J. Bard, L.R. Faulkner, Electrochemical Methods: Fundamentals and Applications, Wiley, 1980.
[113] M. Favaro, B. Jeong, P.N. Ross, J. Yano, Z. Hussain, Z. Liu, E.J. Crumlin, Unravelling the electrochemical double layer by direct probing of the solid/liquid interface, Nat. Comm. 7 (2016) 12695.
[114] Y.C. Wen, S. Zha, X. Liu, S. Yang, P. Guo, G. Shi, C. Tian, Unveiling microscopic structures of charged water interfaces by surface-specific vibrational spectroscopy, Phys. Rev. Lett. 116 (2016) 016101.
[115] D.M. Itkis, J.J. Velasco-Velez, A. Knop-Gericke, A. Vyalikh, M.V. Avdeev, L. Yashina, Probing operating electrochemical interfaces by photons and neutrons, ChemElectroChem 2 (2015) 1427–1445.
[116] K. Ataka, T. Yotsuyanagi, M. Osawa, Potential-dependent reorientation of water molecules at an electrode/electrolyte interface studied by surface-enhanced infrared absorption spectroscopy, J. Phys. Chem. 100 (1996) 10664–10672.
[117] M. Fleischmann, P.J. Hendra, I.R. Hill, M.E. Pemble, Enhanced Raman spectra from species formed by the coadsorption of halide ions and water molecules on silver electrodes, J. Electroanal. Chem. 117 (1981) 243–255.
[118] Y.R. Shen, V. Ostroverkhov, Sum-frequency vibrational spectroscopy on water interfaces: polar orientation of water molecules at interfaces, Chem. Rev. 106 (2006) 1140–1154.
[119] A. Knop-Gericke, V. Pfeifer, J.J. Velasco-Velez, T. Jones, R. Arrigo, M. Hävecker, R. Schlögl, In, situ X-ray photoelectron spectroscopy of electrochemically active solid-gas and solid-liquid interfaces, J. Elect. Spec. Rel. Phen. 221 (2017) 10–17.
[120] J.J. Velasco-Velez, M. Hävecker, A. Knop-Gericke, C. Schwanke, L. Xi, K.M. Lange, J. Xiao, M.F. Tesch, R. Golnak, P. Tristan, L. Puskar, U. Schade, M. Borgwardt, I. Kiyan, R. Scheidel, E.F. Aziz, Multiscale photo-based in-situ and operando spectroscopies in time and energy landscapes, Synch. Rad. News 30 (2017) 14–19.
[121] A. Klyushin, R. Arrigo, V. Pfeifer, T. Jones, J.J. Velasco-Velez, A. Knop-Gericke, Catalyst electronic surface structure under gas and liquid environments, encyclopedia of interfacial, Chem.: Surf. Sci. Electrochem. (2018) 615–631.
[122] A. Nilsson, D. Nordlund, I. Waluyo, N. Huang, H. Ogasawara, S. Kaya, U. Bergmann, L.A. Näslund, H. Öström, Ph. Wernet, K.J. Andersson, X-ray absorption spectroscopy and X-ray Raman scattering of water and ice; an experimental view, J. Electron Spectros. Relat. Phen. 177 (2010) 99–129.
[123] H. Bluhm, D.F. Ogletree, C.S. Fadley, Z. Hussain, M. Salmeron, The premelting of ice studied with photoelectron spectroscopy, J. Phys. Condens. Matter 14 (2012) L227–L233.
[124] A. Nilsson, L.G.M. Pettersson, Chemical bonding on surfaces probed by X-ray emission spectroscopy and density functional theory, Surf. Sci. Rep. 55 (2004) 49–167.
[125] T. Tokushima, Y. Horikawa, H. Arai, Y. Harada, O. Takahashi, L.G.M. Pettersson, A. Nilsson, S. Shin, Polarization dependent resonant X-ray emission spectroscopy of D_2O and H_2O water: assignment of the local molecular orbital symmetry, J. Chem. Phys. 136 (2012) 044517.
[126] P. Jiang, J.L. Chen, F. Borondics, P.A. Glans, M.W. West, C.L. Chang, M. Salmeron, J. Guo, In situ soft X-ray absorption spectroscopy investigation of electrochemical corrosion of copper in aqueous $NaHCO_3$ solution, Electrochem. Commun. 12 (2010) 820–822.
[127] J.J. Velasco-Vélez, T.E. Jones, V. Pfeifer, C.L. Dong, Y.X. Chen, C.M. Chen, H.Y. Cheng, Y.R. Lu, J.M. Chen, R. Schlögl, A. Knop-Gericke, C.H. Chuang, Trends in reactivity of electrodeposited 3d transition metals on gold revealed by operando soft X-ray absorption spectroscopy during water splitting, J. Phys. D: Appl. Phys. 50 (2016) 024002.
[128] J.J. Velasco-Velez, C.H. Chuang, H.L. Han, I. Martin-Fernandez, C. Martinez, W.F. Pong, Y.R. Shen, F. Wang, Y. Zhang, J. Guo, M. Salmeron, In-situ XAS investigation of the effect of electrochemical reactions on the structure of graphene in aqueous electrolytes, J. Electrochem. Soc. 160 (2013) C445–C450.
[129] J.J. Velasco-Velez, C.H. Wu, B.Y. Wang, Y. Sun, Y. Zhang, J.H. Guo, M. Salmeron, Polarized X-ray absorption spectroscopy observation of electronic and structural changes of chemical vapor deposition graphene in contact with water, J. Phys. Chem. C 118 (2014) 25456–25459.
[130] J.J. Velasco-Velez, C.H. Wu, T. Pascal, L.F. Wan, J. Guo, D. Prendergast, M. Salmeron, The structure of interfacial water on gold electrodes studied by X-ray absorption spectroscopy, Science 346 (2014) 831–834.
[131] J.J. Velasco-Velez, V. Pfeifer, M. Hävecker, R.S. Weatherup, R. Arrigo, C.H. Chuang, E. Stotz, G. Weinberg, M. Salmeron, R. Schlögl, A. Knop-Gericke, Photoelectron spectroscopy at the graphene–liquid interface reveals the electronic structure of an electrodeposited cobalt/graphene electrocatalyst, Ang. Chem. Int. Ed. 54 (2015) 14554–14558.
[132] A. Kolmakov, D.A. Dikin, L.J. Cote, J. Huang, M.K. Abyaneh, M. Amati, L. Gregoratti, S. Günther, M. Kiskinova, Graphene oxide windows for in situ environmental cell photoelectron spectroscopy, Nature Nanotech. 6 (2011) 651.
[133] D. Prendergast, G. Galli, X-ray absorption spectra of water from first principles calculations, Phys. Rev. Lett. 96 (2006) 215502.
[134] U. Bergmann, Ph. Wernet, P. Glatzel, M. Cavalleri, L.G.M. Pettersson, A. Nilsson, S.P. Cramer, X-ray Raman spectroscopy at the oxygen K edge of water and ice: implications on local structure models, Phys. Rev. B 66 (2002) 092107.
[135] S. Axnanda, E.J. Crumlin, B. Mao, S. Rani, R. Chang, P.G. Karlsson, M.O.M. Edwards, M. Lundqvist, R. Moberg, P. Ross, Z. Hussain, Z. Liu, Using "Tender" X-ray ambient pressure X-ray photoelectron spectroscopy as a direct probe of solid-liquid interface, Sci. Rep. 5 (2015) 9788.
[136] M. Favaro, W.S. Drisdell, M.A. Marcus, J.M. Gregoire, E.J. Crumlin, J.A. Haber, J. Yano, An operando investigation of (Ni-Fe-Co)O_x system as highly efficient electrocatalyst for oxygen evolution reaction, ACS Catal. 7 (2) (2017) 1248–1258.
[137] M. Favaro, F. F: Lamers, E. J. Crumlin, Z. Liu, R. van de Krol, D. Starr, Light-induced surface reactions at the bismuth vanadate/potassium phosphate interface, J. Phys. Chem. B. 122 (2) (2018) 801–809.
[138] S. Nappini, A. Matruglio, D. Naumenko, S. Dal Zilio, F. Bondino, M. Lazzarino, E. Magnano, Graphene nanobubbles of TiO_2 for in-operando electron spectroscopy of liquid-phase chemistry, Nanoscale 9 (2017) 4456–4466.